5

Accoustic Wave

P. K. Karmakar
Department of Physics, Tezpur University, Napaam, Tezpur, Assam
India

1. Introduction

An acoustic wave basically is a mechanical oscillation of pressure that travels through a medium like solid, liquid, gas, or plasma in a periodic wave pattern transmitting energy from one point to another in the medium [1-2]. It transmits sound by vibrating organs in the ear that produce the sensation of hearing and hence, it is also called acoustic signal. This is well-known that air is a fluid. Mechanical waves in air can only be longitudinal in nature; and therefore, all sound waves traveling through air must be longitudinal waves originating in the transmission form of compression and rarefaction from vibrating matter in the medium. The propagation of sound in absence of any material medium is always impossible. Therefore, sound does not travel through the vacuum of outer space, since there is nothing to carry the vibrations from a source to a receiver. The nature of the molecules making up a substance determines how well or how rapidly the substance will carry sound waves. The two characteristic variables affecting the propagation of acoustic waves are (1) the inertia of the constituent molecules and (2) the strength of molecular interaction. Thus, hydrogen gas, with the least massive molecules, will carry a sound wave at 1,284.00 ms^{-1} when the gas temperature is 0^0 C [1]. More massive helium gas molecules have more inertia and carry a sound wave at only 965.00 ms^{-1} at the same temperature. A solid, however, has molecules that are strongly attached, so acoustic vibrations are passed rapidly from molecule to molecule. Steel, for an instant example, is highly elastic, and sound will move rapidly through a steel rail at 5,940.00 ms^{-1} at the same temperature. The temperature of a medium influences the phase speed of sound through it. The gas molecules in warmer air thus have a greater kinetic energy than those of cooler air. The molecules of warmer air therefore transmit an acoustic impulse from molecule to molecule more rapidly. More precisely, the speed of a sound wave increases by 0.60 ms^{-1} for each Celcius degree rise in temperature above 0^0 C.

Acoustic waves, or sound waves, are defined generally and specified mainly by three characteristics: wavelength, frequency, and amplitude. The wavelength is the distance from the top of one wave's crest to the next (or, from the top of one trough to the next). The frequency of a sound wave is the number of waves that pass a point each second [1]. Sound waves with higher frequencies have higher pitches than sound waves with lower frequencies and vice versa. Amplitude is the measure of energy in a sound wave and affects volume. The greater the amplitude of an acoustic wave, the louder the sound and vice versa. An acoustic wave is what makes humans and other animals able to hear. A person's ear perceives the vibrations of an acoustic wave and interprets it as sound [1]. The outer ear, the visible part, is shaped like a funnel that collects sound waves and sends them into the ear

canal where they hit the ear drum, which is a tightly stretched piece of skin that vibrates in time with the wave. The ear drum starts a chain reaction and sends the vibration through three little bones in the middle ear that amplify sound. Those bones are called the hammer, the anvil, and the stirrup.

Furthermore, acoustic waves from a purely hydrodynamic point of view are small-amplitude disturbances that propagate in a compressible medium (like a fluid) through the interplay between fluid inertia, and the restoring force of fluid pressure. The propagation of small-amplitude disturbances in homogeneous medium is observed as acoustic waves such as water waves, and in self-gravitationally stratified medium like stellar atmosphere [36-37, 41-44], acoustic-gravity waves such as p-modes, g-modes, f-modes, etc., as found by helio- and astero-seismological studies. Acoustic waves propagating through a dispersive medium may get dynamically converted into *solitons* or *shocks* depending on the physical mechanisms responsible for their saturation. When fluid nonlinearity (convective effect) is balanced by dispersion (geometrical effect), solitons usually result [4]. Conversely, shocks are formed if fluid nonlinearity is balanced by dissipation (damping effect). The nonlinear hydrodynamic equations of various forms (like KdV equation, Burger equation, NLS equation, BO equation, etc.) in the context of the generation, structure, propagation, self-organization and dissipation of solitons or shocks have long been developed applying the hydrodynamic views of the usual conservation laws of flux, momentum and energy [4]. Similar outlook is needed to understand the formation of other nonlinear localized structures of low frequency acoustic waves like double layers, vortices, etc. They are important in a wide variety of space, astrophysical and laboratory problems for the investigation of dynamical stability against perturbation [3-4]. In addition, these equations have wide applications to study a nonlinear, radial, energetic, and steady-flow problem that provides a first rough approximation to the physics of stellar winds and associated acoustic wave kinetics, which are responsible for stellar mass-loss phenomena via supersonic flow into interstellar space [2].

Acoustic mode in plasmas of all types [2-44], similarly, is actually a pressure driven longitudinal wave like the ordinary sound mode in neutral gas. In normal two-component plasmas, the electron thermal pressure drives the collective ion oscillations to propagate as the ion sound (acoustic) wave. Here the electron thermal pressure provides the restoring force to allow the collective ion dynamics in the form of ionic compression and rarefaction to propagate in the plasma background and ionic mass provides the corresponding inertial force. Thermal plasma species (like electrons) are free to carry out thermal screening of the electrostatic potential. In absence of any dissipative mechanism, the ion sound wave moves with constant amplitude. For mathematical description of the ion sound kinetics, the plasma electrons are normally treated as inertialess species and the plasma ions, with full inertial dynamics. However, recent finding of ion sound wave excitation in *transonic plasma* condition of hydrodynamic equilibrium offers a new physical scope of acoustic turbulence due to weak but finite electron inertial delay effect [5-12]. Qualitative and quantitative modifications are introduced into its nonlinear counterpart as well, under the same transonic plasma equilibrium configuration [12]. The *transonic transition* of the plasma flow motion quite naturally occurs in the neighborhood of boundary wall surface of laboratory plasmas, self-similar expansion of plasmas into vacuum, in solar wind plasmas and different astrophysical plasmas, etc. The self-similar plasma expansion model predicts supersonic motion of plasma flow into vacuum. This model is widely used to describe the motion of intense ion plasma jets produced by short time pulse laser interaction with solid target [17-

23]. Recently, the self-similar plasma expansion into vacuum is modeled by an appropriate consideration of space charge separation effect on the expanding front [13].

According to the recently proposed inertia-induced ion acoustic excitation theory [5-8], the large-scale plasma flow motion feeds the energy to the short scale fluctuations near the pre-sheath termination at sonic point. This is a kind of energy transfer process from large-scale flow energy to wave energy through short scale instability of cascading type. In order to maintain the turbulence type of hydrodynamic equilibrium, there must be some source to feed large-scale flow and sink to arrest the infinite growth of the excited short waves. The growing wave energy could be used to re-modify the global transonic equilibrium such that the transonic transition becomes a natural equilibrium with smooth change in flow motion from subsonic to supersonic regime. Of course, this is a quite involved problem to handle the self-consistent turbulence theory of transonic plasma in terms of anomalous transport [5]. Now one may ask how to produce such boundary layer with sufficient size of the transonic plasma layer for laboratory experimentations?

This, in fact, is an experimental challenge to design and set up such experiments to produce extended length of the transonic zone to sufficient extent to resolve the desired unstable wave spectral components. Creation of a thick boundary layer of transonic flow dynamics is, no doubt, an important task. This zone lies between subsonic and supersonic domains, and is naturally bounded by low supersonic and high subsonic speeds. It should be mentioned here that the sonic velocity corresponds to the phase velocity of the bulk plasma mode of the dispersionless ion acoustic wave. In case of sheath edge boundary, transonic layer could be probed by high-resolving diagnosis of the Debye length order. The desired experiments of spectral analysis of the unstable ion acoustic waves in *transonic plasma condition* may be quite useful to resolve the mystery of sheath edge singularity. Using *de-Lavel nozzle mechanism* of hydrodynamic flow motion, experiments could be designed to produce transonic transition layer of desired length and characteristics [6-8].

Study of the ambient acoustic spectrum associated with plasma flow motion can be termed as the *acoustic spectroscopy* of equilibrium homogeneous plasma flows [6, 26]. This may be useful for expanding background plasmas [13], solar wind plasmas and also in space plasmas through which the space vehicles' motion and aerodynamic motion occur [3, 25, 28]. Basic principles of the acoustic spectroscopy have concern to the linear and non-linear ion acoustic wave turbulence theory and properties of the transonic plasma equilibrium [5-12, 26]. These properties may be used to develop the required diagnostic tools to study and describe the hydrodynamic equilibrium states of plasma flows by suitable observations and analysis of the waves and instabilities they exhibit. In fact, the ambient turbulence-driven plasma flow is quite natural to occur in toroidal and poloidal directions of the magnetic confinement of tokamak device. Similar physical mechanism is supposed to be operative in the transonic transition behavior of equilibrium plasma flow motion [5-12]. Thorough investigations of acoustic wave turbulence theory in transonic plasma condition will be needed to explore transonic flow dynamics on a concrete footing.

Recently, there has been an outburst of interest in plasma states where the assumption of static equilibrium practically is violated [28-30]. Great deals of research activities are now going on in transonic and supersonic magnetohydrodynamic (MHD) flows in laboratory and astrophysical plasmas. Similar activities are also important for understanding the designing of supersonic aerodynamics having relevance in spacecraft-based laboratory

experimentations of space plasma research as well [8, 30]. This is also argued that future tokamak reactors need the consideration of rotation of fusion plasma with high speeds that do not permit the assumption of static equilibrium to hold good. This may be brought about due to neutral beam heating and pumped divertor action for the extraction of heat and exhaust.

In astrophysics [3, 28-32, 35-44], the primary importance of plasma flows is revealed in such diverse situations as coronal flux tubes, stellar winds, rotating accretion disks, torsional modes, and jets emitted from radio galaxies. This is to argue that the basic understanding of the acoustic wave dynamics in transonic plasma system constitutes an important subject of future interdisciplinary research [5-12, 26-30]. This may be useful for development of the appropriate diagnostics for acoustic spectroscopy to measure and characterize the hydrodynamic equilibrium of flowing transonic plasmas [8-10]. Such concepts of acoustic wave dynamics in a wider horizon may also applied to understand some helio- and astero-seismic observations in astrophysical contexts.

Most of the plasma devices of industrial applications like dense plasma focus machine, plasma torches, etc. depend on the plasma flows that violate the static equilibrium [26-30]. In fusion plasmas of future generation too, the static approximation of the equilibrium plasma description may not be suitable to describe the acoustic wave behavior. In future course of fusion research, rotational motions of fusion plasmas in poloidal and toroidal directions may decide the equilibrium. This is important to state that in toroidal plasmas, the geodesic acoustic mode becomes of fundamental importance in comparison to the ordinary sound modes [30]. This may be more important when these rotational motions are in the defined range of the transonic limit. Simplicity is correlated to the local mode approximation of the acoustic wave description in transonic limit of uniform and unidirectional plasma flow motion without magnetic field.

The lowest order nonlinear wave theory of the ion acoustic wave dynamics predicts that the usual KdV equation is not suitable to describe the kinetics of the nonlinear traveling ion acoustic waves in transonic plasma condition [8-9, 12, 26]. A self-consistent linear source driven KdV equation, termed as *d*-KdV equation, is prescribed as a more suitable nonlinear differential equation to describe the nonlinear traveling ion acoustic wave dynamics in transonic plasma condition. By mathematical structure of the derived *d*-KdV equation, it looks analytically non-integrable and physically non-conservative dynamical system [8-9]. Due to linear source term, an additional class of nonlinear traveling wave solution of oscillatory shock-like nature is obtained. This is more prominent in the shorter scale domain of the unstable ion acoustic wave spectrum, but within the validity limit of weak nonlinearity and weak dispersion.

If there is multispecies ionic composition in a plasma system, varieties of plasma sound waves are likely to exist depending on, in principle, the number of inertial ionic species. In plasmas containing two varieties of dust or fine suspended particles, two distinct kinds of natural plasma sound modes are possible [15-16]. Such plasmas, termed as the *colloidal plasmas* [16], have become the subject of intensive study in various fields of physics and engineering such as in space, astrophysics, plasma physics, plasma-aided manufacturing technique, and lastly, fusion technology [14-23]. The dust grains or the solid fine particles suspended in low temperature gaseous plasmas are usually negatively charged. It is also observed that plasmas including micro scale-sized and nano scale-sized suspended particles exist in many natural conditions of technological values. Such plasmas have been generated in laboratories with a view to investigate the dust grain charging physics, plasma wave physics as well as some acoustic instability phenomena.

The two distinct sound modes, however, in bi-ion colloidal plasma are well-separated in space and time scales due to wide range variations of mass scaling of the normal ions and the charged dust grains and free electrons' populations. The charged dust grains are termed as the *Dust Grain Like Impurity Ions* (DGLIIs) [15] to distinguish from the normal impurity ions. The present contributory chapter, additionally, applies the inertia-induced acoustic excitation theory to nonlinear description of plasma sound modes in colloidal plasma [15-16] under different configurations. Two separate cases of ion flow motion and dust grain motions are considered. It is indeed found that the *modified Ion Acoustic Wave* (m-IAW) or *Dust Ion Acoustic* (DIA) *wave* and the *so-called (Ion) Acoustic Wave* (s-IAW) or *Dust Acoustic* (DA) *wave* both become nonlinearly unstable due to an active role of weak but finite inertial correction of the respective plasma thermal species [15, 26]. Proper mass domain scaling of the dust grains for acoustic instability to occur is estimated to be equal to that of the asymptotic mass ratio of plasma electron to ion as the lowest order inertial correction of background plasma thermal species. This contributory chapter is thus a review organized to aim at some illustrative examples of linear and nonlinear acoustic wave propagation dynamics through transonic plasma fluid, particularly, under the light of current scenario. Some important reported findings on nonlinear acoustic modes found in space and astrophysical situation [31-44], like in solar plasma system [10-11, 31-44], will also be presented in concise to understand space phenomena. Incipient future scopes of the presented contribution on transonic flow dynamics in different astrophysical situations will also be briefly pointed out.

2. Physical model description

A simple two-component non-isothermal, field-free and collisionless plasma system under fluid limit approximation is assumed. The plasma ions are supposed to be drifting with uniform velocity at around the sonic phase speed under field-free approximation. Global plasma equilibrium flow motion over transonic plasma scale length at hydrodynamic equilibrium is assumed to satisfy the global quasi-neutrality. Such situations are realizable in the transonic region of the plasma sheath system as well as in solar and other stellar wind plasmas [3, 10-11, 35-41]. Its importance has previously been discussed [1, 5-12], where the ion-beam driven wave phenomena are supposed to be involved in *Q*-machine or in unipolar/ bipolar ion rich sheath formed around an electrode wall or grid in Double Plasma Device (DPD) experiments of plasma sheath driven low frequency instabilities of relaxation type [5]. The unstable situation is equally likely to occur on both the sides of the sheath structures with plasma ion streamers [12].

3. Linear normal acoustic mode analyses

3.1 Basic governing equations

The basic set of governing dynamical evolution equations for the linear normal mode behavior of fluid acoustic wave consist of electron continuity equation, electron momentum equation, ion continuity equation, and ion momentum equation [5-6]. The set is closed by coupling the plasma thermal electron dynamics with that of plasma inertial ion dynamics through a single Poisson's equation for electrostatic potential distribution due to localized ambipolar effects. Applying Fourier's wave analysis for linear normal mode behavior of ion acoustic wave over the basic set of governing dynamical evolution equations [5-6], the linear dispersion relation is derived as follows

$$(\Omega + k.v_0)^2 = \frac{k^2 v^2_{te}\left(1 + k^2 \lambda^2_{De}\right)}{\Omega^2}\left(\Omega_a^2 - \Omega^2\right). \quad (1)$$

All the notations in the equation (1) are usual and conventional. Here Ω is the Doppler-shifted frequency of the ion acoustic wave, Ω_a is the ion acoustic wave frequency in laboratory frame of reference, k is the angular wave number of the ion acoustic wave such that $k\lambda_{De}$ is a measure of the acoustic wave dispersion scaling and v_{te} is the electron thermal velocity. Now the kinematics of any mode can be analyzed in two different ways: one in lab-frame and the other, in Doppler-shifted frame of reference. This is to note that the obtained dispersion relation differs from those of the other known normal modes of low frequency relaxation type of instability, ion plasma oscillations and waves. This is due to the weak but finite electron inertial delay effect in the dispersion relation of the wave fluctuations. This is mathematically incorporated by a weak inertial perturbation over electron inertial dynamics over the leading order solution obtained by virtue of electron fluid equations neglecting electron inertial term.

It is thus obvious from the mathematical construct of equation (1) that the LHS is a non-resonant term whereas RHS is a resonant term. The RHS gets artificially transformed into a resonant term if and only if $k.v_{i0} < 0$. Now, it can be inferred that equation (1) represents a resonantly unstable situation at Doppler shifted resonance frequency of $\Omega \approx |k.v_0| \geq \Omega_a$, if and only if $k.v_0$ <0. This means that only the mode counter moving with respect to the plasma beam mode gets resonantly unstable. The resonance growth rate for this resonant instability [5-6] is found to be of the following form

$$\gamma = \sqrt{\frac{m_i}{m_e} 2\Omega_a}\left(1 + k^2 \lambda_{De}^2\right)\left|\left(\Omega - |k.v_0|\right)^{1/2}\right|. \quad (2)$$

This is important to add that the resonance condition required by equation (1) dictates the propagation direction of the unstable ion acoustic wave (counter moving with respect to plasma ion streams) at reduced frequencies. It is clear from equation (2) that there is the physical appearance of two distinct classes of eigen mode frequencies of the resonantly coupled mode-mode system of linearly growing ion acoustic oscillations in lab-frame: near-zero frequency (standing mode pattern) and non-zero frequency (propagating mode pattern). These two distinct eigen modes are generated by the process of repeated Doppler-shifting of the ion acoustic wave frequency under the unique mathematical compulsion of the hydrodynamic tailoring of the electron fluid density perturbation over ion acoustic time scale. The unstable condition decides the resonant acoustic excitation threshold value for the onset of the instability in terms of normalized value of the eigen mode frequency of the acoustic fluctuations.

3.2 Graphical analysis

It is well-known that the graphical method is a more informative, simple and quick tool for analyzing the stability behavior of a plasma-beam system even without solving dispersion relation. To depict the clear-cut picture of the poles, relation (1) is rewritten as,

$$F(\Omega, k) = \frac{1}{\left(1 + k^2 \lambda_{De}^2\right)} = k^2 v_{te}^2 \left[\frac{\Omega_a^2}{\Omega^2 (\Omega + k.v_0)^2} - \frac{1}{(\Omega + k.v_0)^2}\right]. \quad (3)$$

It is clear from the equation (3) that two poles are possible to exist in Ω-space at $\Omega = 0$ and $\Omega = |k.v_0|$ for $k.v_0 < 0$. According to graphical method, the beam-plasma system will exhibit instability only when the curve of $F(\Omega,k)$ versus Ω has multiple singular values in Ω-space having finite minima in between the two successive singularities, which do not intersect with the line $F(\Omega,k) = 1/\left(1+k^2\lambda_{De}^2\right)$. The required condition for minimization of $F(\Omega,k)$ in Ω-space can be obtained by equating $dF/d\Omega = 0$. Now this condition, when applied to equation (3), results into the following equality to derive the value of Ω where dispersion function is supposed to be minimum

$$\Omega_a^2\left(\Omega + k.v_0\right) + \Omega\left(\Omega_a^2 - \Omega^2\right) = 0. \tag{4}$$

In principle, equation (4) is to be solved to determine the value of Ω. This is obvious to note that this equality is satisfied at resonance value of $\Omega \sim |k.v_0| \sim \Omega_a$ for $k.v_0 < 0$. Now to indemnify the complex nature of Ω, the functional value of $F(\Omega,k) > 1/\left(1+k^2\lambda_{De}^2\right)$. This can, however, be further simplified to yield the following inequality to determine the threshold value for the onset of the inertia-induced instability

$$k^2 v_{te}^2\left(\Omega_a^2 - \Omega^2\right) > \left(\Omega - |k.v_0|\right)^2 \Big/ \left(1+k^2\lambda_{De}^2\right). \tag{5}$$

The threshold condition for the instability is satisfied for equality sign at resonance frequency $\Omega \sim |k.v_0| \sim \Omega_a$ that characterizes the case of a marginal instability. A few typical plots of the function $F(\Omega,k)$ in Ω-space for shorter and longer acoustic wavelengths (perturbation scale lengths) are represented in Fig. 1.

3.3 Numerical analysis

Numerical techniques for solving polynomials over years have developed to a vast extent for solving polynomials even with complex coefficients and complex variables. For the present case, the Laguerre's algebraic root-finding method [6] to solve the normalized form of polynomial equation has been used. The polynomial $P\left(\Omega'\right)$ in the normalized form of the dispersion relation (1) in ion-beam frame is given below

$$P\left(\Omega'\right) = a_0 + a_1\Omega' + a_2\Omega'^2 + a_3\Omega'^3 + a_4\Omega'^4 = 0. \tag{6}$$

Here all the normalized notations used are usual, generic and defined by $\Omega' = \Omega/\omega_{pi}$, $\Omega_a' = \Omega_a/\omega_{pi}$ $k' = k\lambda_{De}$, $v'_{te} = v_{te}/c_s = \sqrt{m_i/m_e}$ and $M = v_0/c_s$. The expressions for the various coefficients in the polynomial $P\left(\Omega'\right)$ are defined as follows

$$a_0 = -\left(1+k'^2\right)\left(k'^2 v_{te}'^2 \Omega_a'^2\right),$$

$$a_1 = 0,$$

$$a_2 = \left(|k'.M|\right)^2 + \left(1+k'^2\right)\left(k'^2 v_{te}'^2\right),$$

$$a_3 = -2|k'.M|, \text{ and}$$

$$a_4 = 1 .$$

It is found that out of four possible roots of $P(\Omega')$, only two roots are complex and these are the complex conjugates as a pair. For all the complex conjugated roots, only the complex root with positive imaginary part is useful, since this determines the growth rate of the instability. Real and imaginary parts of the corresponding complex roots are then plotted as shown in Figs. 2 and 3, respectively. Numerical characterization of the unstable mode of the instability clearly depicts the resonant character of the electron inertia-induced resonant acoustic instability [5].

3.4 Evaluation of wave energy

This is important to evaluate the wave energy in order to have a more complete picture of the basic source mechanism of the discussed instability. In presence of the beam, it is expected that one of the modes involved, has positive energy and the other has negative energy. The dispersion relation (1) can be put in the laboratory frame for a more clear identification and characterization of the positive and negative energy modes in the form of dispersion function $\varepsilon(\omega,k)$ as follows

$$\varepsilon(\omega,k) = 1 + \frac{1}{k^2\lambda_{De}^2}\left(1 + \frac{{\omega_{pe}}^2}{k^2 v_{te}^2}\right) - \frac{\omega_{pi}^2}{(\omega - k.v_0)^2} = 0. \tag{7}$$

The average electric field energy stored in a propagating electrostatic (created by ambipolar effect) wave in a medium is given by the following relation [6]

$$W_\omega(\omega,k) = \frac{1}{2}\varepsilon_0 \left\langle \left|\delta E(\omega,k)\right|^2 \right\rangle \frac{\partial}{\partial\omega}\left[\omega\varepsilon(\omega,k)\right]. \tag{8}$$

Here ε_0 is the dielectric constant of free space, $\delta E(\omega,k)$ is the electric field amplitude of the ion acoustic fluctuations and $W_E = 1/2\left|\delta E(\omega,k)\right|^2$ is the corresponding counterpart of electric energy of the acoustic fluctuations through free space. Applying the equations (7) and (8), the following can explicitly be derived

$$\frac{W_\omega}{W_E} = \omega\frac{\partial\varepsilon(\omega,k)}{\partial\omega} = \left[\frac{2\omega^2}{k^2\lambda_{De}^2 k^2 v_{te}^2} + \frac{2\omega\omega_{pi}^2}{(\omega - k.v_0)^3}\right]. \tag{9}$$

Now, clearly, it is evident that the second term of equation (9) contributes negative energy value to the defined wave-plasma system. This occurs as because the sign of this term becomes negative for the values of $\omega < k.v_0$, which is the case for the reported instability. From a few typical plots in Fig.4, one can notice that the total wave energy suffers a sharp transition from negative to positive values at resonance frequency point of zero energy value. The resonance point lies in the domain of near-zero and non-zero frequencies in lab-frame. According to conventional definition and understanding, the wave energy expression in equation (9) classifies the near-zero frequency mode as the negative energy mode. Then immediately the non-zero frequency mode may be classified as the positive energy mode.

This is important to clarify that the theoretical concept of near-zero frequency mode is an outcome of the mathematical construct of weak but finite electron inertial response to the ion acoustic wave fluctuations. The blowing up character, as shown in Fig. 4, of the total wave energy in opposite directions suggests referring the discussed instability to as an 'explosive instability' in accordance with the law of conservation of energy. It signifies the transonic plasma condition with the resonant mode-mode coupling of the positive and negative energy modes. The time average of the hydrodynamic and wave potential energies of the considered wave-plasma system over the growth time scale is conserved during the energy exchange process between the unstable resonant eigen modes and the main source of ion flow dynamics. These two modes are clearly identified from equation (9) as the natural resonant modes of the defined plasma system that undergo linear resonant mode-mode coupling to produce the defined wave instability.

3.5 Estimation of quenching time

Under the cold ion approximation, even the small electrostatic potential will be able to distort the ion particle motion and associated trajectories, affecting the driving source flow velocity of the resonant instability under consideration. In wave frame, the streaming ion energy (E_i) can be expressed by the following relation

$$E_i = \frac{1}{2} m_i \left(v_0 - \frac{\omega}{k} \right)^2 . \tag{10}$$

For $v_o >> \omega/k \sim |(c_s - v_0)|$, which is a valid case for the considered instability [5], the condition for ion orbit distortion becomes of the following form,

$$W_w \geq \frac{1}{2} m_i n_0 v_0^2 . \tag{11}$$

From this condition, the quenching time is estimated under the assumption that the wave amplitude grows sufficiently from thermal noise level to physically measurable level such that

$$W_E(t) = W_i e^{\gamma t} . \tag{12}$$

Here W_i is the initial energy of the acoustic wave amplitude, which is of the order of the thermal fluctuations, i.e., $W_i \sim T_e/\lambda_{De}^3$ and is the unnormalized linear growth rate. Using the resonance values of $\omega = k|c_s - v_0|$ and $\omega - k.v_0 \sim kc_s$ as derived in [5] for long wavelength case of resonant mode, equation (12) for the quenching time τ with the help of (9) can be rewritten as follows

$$\tau = \sqrt{\frac{m_e}{2m_i}} \frac{1}{k\lambda_{De}} \left(|1 - M| \right)^{-1/2} \ln \left[\frac{1}{4} \left(n_0 \lambda_{De}^3 \right) \left(k^2 \lambda_{De}^2 \right) \frac{M^2}{|1 - M|} \right] . \tag{13}$$

For some typical plasma parameters in hydrogen plasma, $\ln\left(n_0 \lambda_{De}^3\right) \sim 15 - 30$. For $k\lambda_{De} \sim 0.3, 0.1, 0.05$ near resonant M as in Figs. 2 and 3, equation (13) gives $\tau > 1$, i.e., $\tau_q > \tau_{pi}$. This physically means that the resonant growth time scale is greater than that of the plasma ion oscillation time scale. Thus the resonant nature of the instability is observable in the present analysis.

3.6 Physical consequences

Wave energy analyses are carried out to depict the graphical appearance of poles (Fig. 1), nature of real parts of the roots (Fig. 2), nature of imaginary parts of roots (Fig. 3) and positive-negative energy modes (Fig. 4).

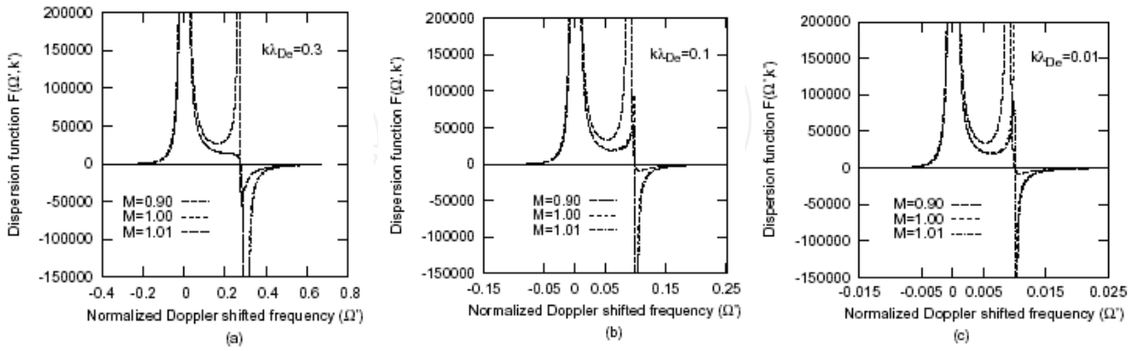

Fig. 1. Graphical appearance of resonance poles as a variation of the dispersion function $F(\Omega,k)$ with normalized Doppler-shifted frequency for dispersion scaling (a) $k\lambda_{De}=0.3$, (b) $k\lambda_{De}=0.1$, and (c) $k\lambda_{De}=0.01$

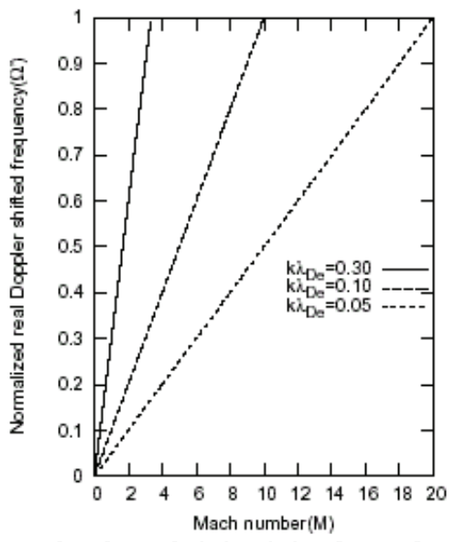

Fig. 2. Variation of the real part of the normalized Doppler shifted eigen mode frequency (Ω') with respect to Mach number (M) for different values of $k\lambda_{De}=0.30,0.10,0.05$

It is found that the instability arises out of linear resonance mode-mode intermixed coupling between the negative and positive energy modes. The total energy of the coupled mode-mode system comprising of hydrodynamical potential energy and wave kinetic energy, however, is in accordance with the law of conservation of energy in the observation time scale on the order of ion acoustic wave time scale. Identification and characterization of the resonance nature of the said instability through *transonic plasma* is presented in order to explore the acoustic richness in terms of collective waves, oscillations and fluctuations. This is an important point to be mentioned here that the same type of instability features are

expected to happen in plasma-wall interaction process and sheath-induced instability phenomena in other similar situations as well.

There are different sorts of analytical and numerical tools for studying the linear instabilities in a given plasma system. *Energy method*, based on energy minimization principle and the *normal mode analysis*, based on equilibrium perturbations are the two basic mathematical tools for analyzing the stability behavior of the given plasma systems. However, the latter is most popular and simple for common use in analyzing the threshold conditions of the instabilities and their growth rates. In the normal mode analysis, a linear dispersion relation is derived which can be put in the form of a polynomial with real or imaginary coefficients. The limitation of the analytical method depends upon the degree of the polynomial.

Computational technique broadly takes into account two ways of investigating instability. First, an unstable mode can be deduced by the derived dispersion relation. The obtained polynomial is then solved to delineate the complex roots having concern to the desired instability. Second, a more comprehensive computational method involves solving for the time dependent solution. Simulation technique used to solve the basic set of equations is supposed to give more complete picture of the space and time evolution of the wave phenomena. However, there is another very informative and simple method for analyzing the derived dispersion relation to predict for the unstable behavior of the plasma system under consideration. This is the graphical method in which the dispersion relation is graphically represented for different values of resonance characterization parameters. Source perturbation scale length $(k\lambda_{De})$ and deviation from sonic point $(1-M)$ are the characterization parameters for the defined acoustic resonance.

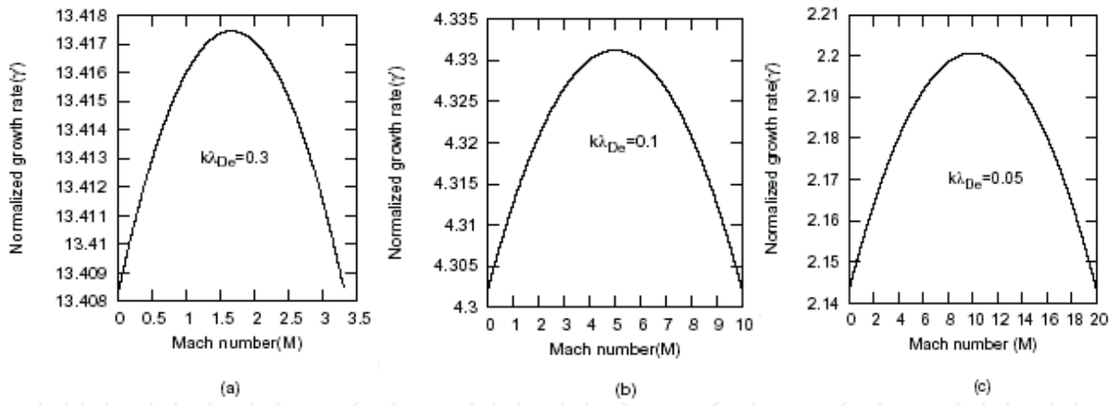

Fig. 3. Variation of the normalized growth rate of the electron inertia-induced resonant acoustic instability with Mach number for (a) $k\lambda_{De}=0.3$, (b) $k\lambda_{De}=0.1$ and (c) $k\lambda_{De}=0.05$ showing that transonic plasma is rich in wide range acoustic spectral components and hence, an unstable zone

This is quite natural and interesting to argue that the transonic plasma condition offers a unique example where the physical situation of localized hydrodynamic equilibrium of quasi-neutral plasma flow dynamics exists. Previous publication reports that the transonic plasma layer, assumed to have finite extension, can be considered as a good physical situation to study the acoustic instability, wave and turbulence driven by electron inertia-induced ion acoustic excitation physics.

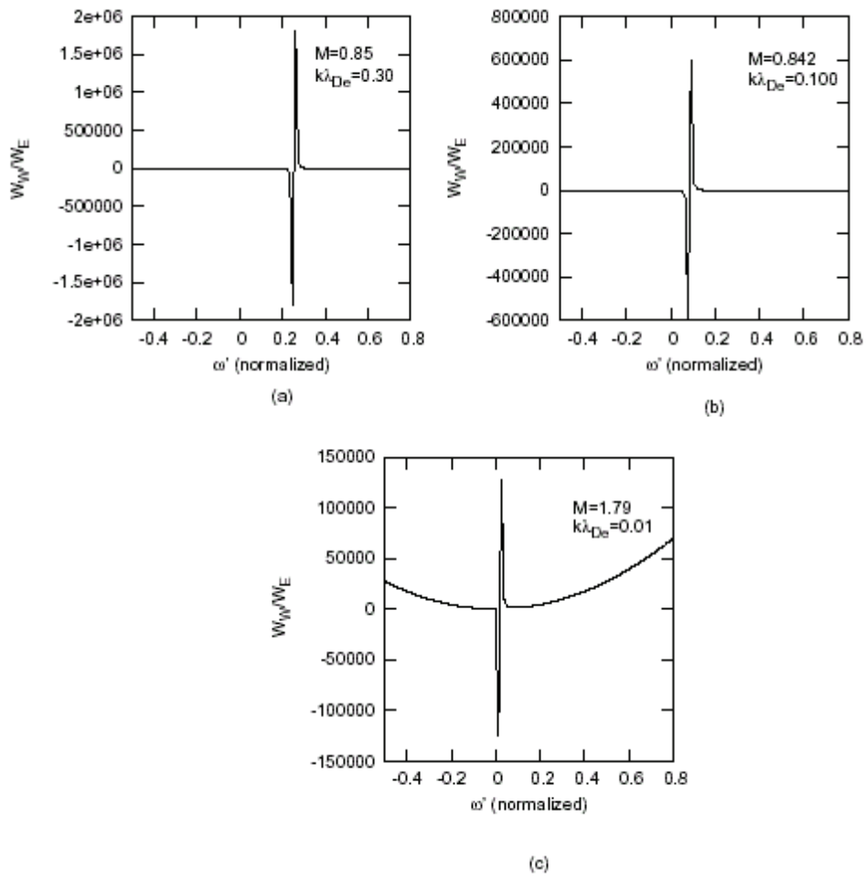

Fig. 4. Explosive nature of the electron inertia-induced ion acoustic wave instability as an outcome of an interplay for the linear resonant mode-mode coupling of positive and negative energy eigen modes. It shows how the normalized wave energy varies with normalized frequency under a set of fixed values of M and $k\lambda_{De}$ as (a) $M = 0.85, k\lambda_{De} = 0.30$; (b) $M = 0.842, k\lambda_{De} = 0.100$; and (c) $M = 1.79, k\lambda_{De} = 0.01$

In the present sections of the chapter, many features about the electron inertia-induced ion acoustic wave instability are observed. For example, we physically identify and demonstrate the following features of the instability obtained by theoretical and numerical means of analysis of the desired dispersion relation:

1. The transonic plasma layer is an unstable zone of hydrodynamic equilibrium of quasineutral plasma gas flow motion,
2. The instability is an outcome of the linear resonant mode-mode coupling of positive and negative energy modes,
3. The quenching time of the instability is estimated for some typical values of plasma and wave parameters as mentioned in the previous section. It is found to moderately exceed the ion plasma oscillation time scale, and
4. Lastly, this indicates that in lab frame observation the unstable mode of ion acoustic wave fluctuations at reduced frequencies may look like a purely growing mode. This is very likely to occur for almost entire unstable frequency domain of the frequency transformed ion acoustic waves.

In fact, the electron inertial responses naturally appear only at electron oscillation frequency. However, the *transonic plasma* condition creates a natural physical situation for the same to occur even at the ion acoustic wave frequency of the transformed reduced values. The linear process of resonant mode-mode coupling produces this and makes the coupled system of wave modes unstable.

We have identified and demonstrated the following features of the instability obtained by theoretical and numerical analysis of the dispersion relation: (i) The transonic plasma layer is indeed an unstable zone of hydrodynamic equilibrium of quasi-neutral plasma gas flow motion. (ii) The instability is an outcome of linear resonant mode-mode coupling of positive and negative energy modes. (iii) The normalized values of Doppler-shifted resonant frequencies of the unstable ion acoustic wave fluctuations in ion beam frame come out to be almost equal to 0.5. (iv) The estimated quenching time of the instability exceeds the ion plasma oscillation time scale moderately and hence, (v) In the lab-frame, the unstable modes of ion acoustic wave fluctuations at reduced frequencies may look physically like a purely growing mode.

This is further argued that the physical insights as listed above can be useful as theoretical, graphical and numerical recipes to (1) formulate and solve the problems of saturation mechanisms of the unstable ion acoustic wave fluctuations, (2) formulate and solve the problems of the ion acoustic wave turbulence, and (3) design and setup experiments to study the basic physics of linear and nonlinear ion acoustic wave activities in unique transonic plasma system. These investigations may be useful to improve the existing conceptual framework of physical and mathematical methods of two-scale theory of plasma sheath research to resolve the long-term mystery of the sheath edge singularity. These, in brief, are added to judge the didactic *vis-à-vis* the scientific qualities of the current research work too much specialized in the subject of ion acoustic wave physics.

3.7 Comments

The main conclusive comment here is that the graphical method successfully explains the unstable behavior of the fluid acoustic mode of the ion acoustic wave fluctuations in drifting plasmas with cold ions and hot electrons. A more vivid picture of linear resonant mode-mode coupling of positive and negative energy waves is obtained. This is important to note that simple formulae for wave energy and quenching time calculations [6] are used. This calculation further confirms the earlier results of stability analysis of drifting plasmas against the acoustic wave perturbations [5]. It is, therefore, reasonable to think of logical hypothesis of wave turbulence model approach to solve the sheath edge singularity problem [1, 4]. Actually, the local normal mode theory of the discussed instability implies that the entire transonic plasma zone should be rich in wide frequency range spectrum of the ion acoustic wave fluctuations. This leads to develop the conceptual framework of *situational definition* of the Debye sheath edge to behave as a turbulent zone with finite extension [12]. This hypothetical scenario of the transonic plasma condition can be examined by appropriate experiments of measuring wide range spectral components of the ion acoustic wave fluctuations.

This is a nontrivial problem to explicitly characterize the turbulent properties of the transonic region. The more realistic problem of wave turbulence analysis demands the self-consistent consideration of flow induced quasi-neutral plasma with inhomogeneity in equilibrium plasma background. Similar situations are likely to occur in stellar wind plasmas, where, the transonic behavior is brought about by *deLaval nozzle mechanism* [6-10]

of gas flow through a tube of varying cross section. Recent experimental observation [12] in double plasma device (DPD) reports an instability even in a condition of symmetric bipotential ion-rich sheath case. Its frequency falls within zero frequency range and its source is believed to lie in presheath.

Finally, in a nutshell, it is concluded that the graphical method of analyzing the dispersion relation of the inertia-induced instability offers a simple and more informative method of practical importance in transonic plasma equilibrium. Moreover, the plasma environment of Debye sheath edge locality offers a realistic situation for self-excitation of the ion acoustic wave turbulence through resonant ion acoustic wave instability. This is induced by hydrodynamic tailoring of the ion acoustic wave-induced electron density fluctuations. Of course, no experimental observation of instability in transonic plasma has yet been reported to directly compare with the theoretical results. However it cannot be undermined in understanding wave turbulence phenomenon of flowing plasmas. This is informative to add that the frequency and amplitude transformation of the normal ion acoustic wave into unstable ion plasma wave at higher frequency is reported in high intense laser–plasma interaction processes [6-7] through the nonlinear ponderomotive action. This leads to the formation of soliton, double layers, etc. through the saturation mechanism of strong laser-plasma interaction processes due to non-zero average value of the spatially varying electric field associated with laser pulse.

4. Nonlinear normal acoustic mode analyses

4.1 Basic governing equations

A large amount of literature of theoretical and experimental investigations has been produced on the solitary wave propagation in plasmas since the theoretical discovery of ion acoustic soliton [4, 11-12, their references]. Varieties of physical situations of drifting ions of high energy with [5-12] and without [13-33] electron inertial correction have been considered in the ion acoustic wave dynamics. It is shown that the electron inertial motion becomes more important than the ion relativistic effect. Such situations exist in Earth's magnetosphere, stellar atmosphere and in Van Allen radiation belts [3]. Similar studies have been carried out in plasmas with additional ion beam fluid with full electron inertial response in motion [12 and references].

A number of experiments were performed in the unstable condition of beam plasma system in laboratory in order to observe soliton amplification [12]. There are many theoretical calculations and experiments on linear [7-8] and nonlinear [9-11] wave propagation properties of acoustic waves to see their behavior near the transonic point. For an assumed transonic region, it has been theoretically shown that the small amplitude acoustic wave fluctuations exhibit linear resonant growth of relaxation type under the consideration of weak but finite electron inertial delay effect [12-13]. In contrast to earlier claim [3] that the complex nature of coefficients in KdV equation prevents the soliton formation, we argue that their interpretation seems to be physically inappropriate. Instead, by global phase modification technique [12], we show that the usual soliton solution exists (even under the unstable condition), but only for infinitely long wavelength source perturbations. Otherwise, oscillatory shock-like solutions are more likely to exist.

Under fluid approximation, the self-consistently closed set of basic dynamical equations for transonic plasma system with all usual notations in normalized form is given as follows

Electron continuity equation:

$$\frac{\partial \phi}{\partial t} + v_e . \frac{\partial \phi}{\partial x} + \frac{\partial v_e}{\partial x} = 0 \text{ , and} \tag{14}$$

Electron momentum equation:

$$\frac{m_e}{m_i}\left(\frac{\partial v_e}{\partial t} + v_e . \frac{\partial v_e}{\partial x} \right) = \frac{\partial \phi}{\partial x} - \frac{1}{n_e}\frac{\partial n_e}{\partial x} . \tag{15}$$

This is to remind the readers that equation (15) is obtained by substituting zero-order solution of Boltzmann electron density distribution into the normal electron continuity equation. In fact, in the asymptotic limit of $m_e/m_i \to 0$, electron continuity equation as such is redundant as because the left hand side (electron inertial effect) of (15) is ignorable. Equation (14) basically offers a scope to introduce the weak but finite role of electron to ion inertial mass ratio on the normal mode behavior of acoustic wave.
Ion continuity equation:

$$\frac{\partial n_i}{\partial t} + \frac{\partial}{\partial x}(n_i v_i) = 0, \tag{16}$$

Ion momentum equation:

$$\frac{\partial v_i}{\partial t} + v_i \frac{\partial v_i}{\partial x} = -\frac{\partial \phi}{\partial x} \text{ , and} \tag{17}$$

Poisson equation:

$$\frac{\partial^2 \phi}{\partial x^2} = n_e - n_i . \tag{18}$$

Following form of the derived *d*-KdV equation obtained from the above equations by the standard methodology of reductive perturbation [12] describes the nonlinear ion acoustic wave dynamics under transient limit (~soliton transit time scale) in a new space defined by the stretched coordinates (ξ, τ). This is to mention that $\phi(x,t) = \phi(\xi,\tau)e^{-\gamma\tau}$ and $\gamma\tau \to 0$ under the transient time action of the propagating ion acoustic soliton through transonic plasma

$$K_0 \frac{\partial \phi}{\partial t} + M_0 \phi \frac{\partial \phi}{\partial x} + \frac{1}{2}\frac{\partial^3 \phi}{\partial x^3} = \gamma K_0 \phi . \tag{19}$$

Here the notations K_0 and M_0 termed as *complex response coefficients* [11-12, 26] and the linear resonant growth rate (γ) of the ion acoustic wave with complex Doppler-shifted Mach number $M_D = M_{Dr} + iM_{Di}$ and lab-frame Mach number $M = M_r + iM_i$ in transonic equilibrium appearing in equation (19) are as follows,

$$K_0 = \left[A^2 + B^2 \right]^{1/2} \text{ where,}$$

$$A=\left(\frac{M_r}{\varepsilon_m}+\frac{M^3{}_{Dr}-3M_{Dr}M_i^2}{\left(M_{Dr}^2+M_i^2\right)^3}\right), \text{ and}$$

$$B=\left(\frac{M_i}{\varepsilon_m}+\frac{M_i^3-3M_{Dr}^2M_i}{\left(M_{Dr}^2+M_i^2\right)^3}\right),$$

$$M_0=\left[C^2+D^2\right]^{1/2} \text{ where,}$$

$$C=\frac{1}{2}\left[\frac{3\left\{\left(M_{Dr}^2-M_i^2\right)^2-4M_{Dr}^2M_i^2\right\}}{\left(M_{Dr}^2+M_i^2\right)^4}-\frac{\left(M_r^2-M_i^2\right)^2-4M_r^2M_i^2}{\varepsilon_m^2}-1\right], \text{ and}$$

$$D=-\frac{1}{2}\left\{\frac{12\left(M_{Dr}^2-M_i^2\right)M_{Dr}M_i}{\left(M_{Dr}^2+M_i^2\right)^4}+\frac{4\left(M_r^2-M_i^2\right)M_rM_i}{\varepsilon_m^2}\right\},$$

$$\gamma=\sqrt{2\left(\frac{m_i}{m_e}\right)}k\lambda_{De}\left|\left(1-v_{i0}\right)^{1/2}\right|.$$

The notations are usual and generic as discussed earlier [12]. In the system, plasma ions are self consistently drifting or streaming through a negative neutralizing background of hot electrons having relatively zero inertia. The time response of the electron fluid here is normally ignored. As a result, the unique role of weak but finite electron inertia to destabilize the plasma ion sound wave in transonic plasma equilibrium even within fluid model approach of normal mode description is masked.

4.2 Physical consequences

Now equation (19) after being transformed into an equivalent stationary ODE form by the Galilean transformations is numerically solved as an initial value problem. Some very small simultaneous values of ϕ, $\partial\phi/\partial\xi$ and $\partial^2\phi/\partial\xi^2$ are required for the numerical programme to proceed. A few numerical plots for the desired nonlinear evolutions are shown in Figs. 5-6. This is to note that the calculated amplitudes (as shown in Figs. 5a-6a) are the solutions of the present *d*-KdV equation (19) with bounded and unbounded phase potraits (as shown in Figs. 5b-6b). Now, the actual amplitudes of the resulting solutions can be deduced by multiplying the numerically obtained values with $\varepsilon\sim\left(k\lambda_{DE}\right)^2\approx10^{-2}$ [12]. In principle, the parameter ε is an arbitrary smallness parameter proportional to the dispersion strength or the amplitude of the weakly dispersive and weakly nonlinear plasma wave.

The unique motivation here is to characterize the possible nonlinear normal mode structure of ion acoustic fluctuations under unstable condition of the ion drifts [8-9,12]. By this very specific example, we show that the complex nature of the coefficients of the derived KdV equation in the unstable zone of transonic plasma doesn't prevent the existence of localized nonlinear solutions including usual soliton solution, too. The concept of global phase

modification technique (DPMT) [11-12, 26] results into a *d*-KdV equation [8-9, 12] with variable nonlinear and dispersion coefficients.

Two distinct classes of solutions are obtained: *soliton* and *oscillatory shock-like* structures. Amplification and damping of the driven KdV soliton over the usual KdV soliton is noted for extremely large wavelength (dc) acoustic driving in source term as shown in Figs. 5-6. The amplification near resonance is associated with considerable reduction in nonlinear coefficient than unity as confirmed by numerical calculation. In other cases of shorter acoustic driving in source term as shown in Figs. 5-6, nonlinear solutions of oscillatory shock-like nature are obtained depending on the small deviation from resonant values. It is clearly seen that the peaks of oscillatory shock-like solutions are of either sinusoidal or non-sinusoidal nature with continuous elevation of the initial values of the successive peaks beyond the main nonlinear acoustic peak.

Most of the experimental results in Double Plasma Device (DPD) are reported to show that the obtained theoretical results may have practical relevance to understand the basic physics of ion acoustic wave activities in the transonic region [12] as in Fig. 7. The experiment is performed in a DPD of 90 *cm* in length and 50 *cm* in diameter equipped with multi-dipole magnets for surface plasma confinement [12]. The chamber is divided into source and target by a mesh grid of 85% transparency kept electrically floating. It is evacuated down to a pressure of $(5-6)\times10^{-5}$ Pa with a turbomolecular pump backed by a rotary pump. *Ar*-gas is bled into the system at a pressure $(3-5)\times10^{-2}$ Pa under continuous pumping condition. The source and target plasmas are produced by dc discharge between the tungsten filament of 0.1 *mm* diameter and magnetic cages.

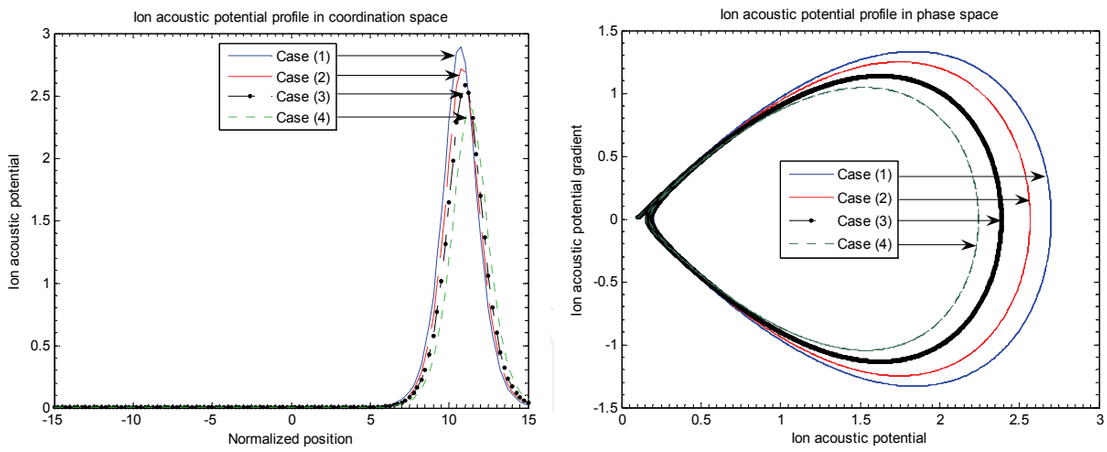

(a) (b)

Fig. 5. Profile of (a) ion acoustic potential (ϕ) with normalized space variable (ξ), and (b) phase space geometry of ion acoustic potential in a phase space described by ϕ and $(\phi)_{\xi}$ with $k\lambda_{De}=2.5\times10^{-8}$ (fixed) for Case (1): $\delta=1.0\times10^{-7}$, Case (2): $\delta=2.5\times10^{-7}$, Case (3): $\delta=5.0\times10^{-7}$, and Case (4): $\delta=7.5\times10^{-7}$

The plasma parameters are measured with the help of a plane Langmuir probe of 5 *mm* diameter and Retarding Potential Analyzer (RPA) of 2.2 *cm* in diameter. The probe and the analyzer are movable axially by a motor driving system so as to take data at any desired

position. The plasma parameters are: electron density $n_0 = 10^8 - 10^9 cm^3$, electron temperature $T_e = 1.0 - 1.5eV$ and ion temperature $T_i = 0.1eV$. An ion-acoustic wave is excited with a positive ramp voltage of which the rise time is controllable and is applied to the source anode of the system. Propagating signals are detected by an axially movable Langmuir probe which is biased to $+4V$ with respect to the plasma potential in order to detect the perturbation in the electron current saturation region. The current is then converted into voltage by a resistance of 100Ω and the resultant signals are fed to the oscilloscope. The probe surface is repeatedly cleaned with ion bombardment by applying $-100V$ to it for a short time scale.

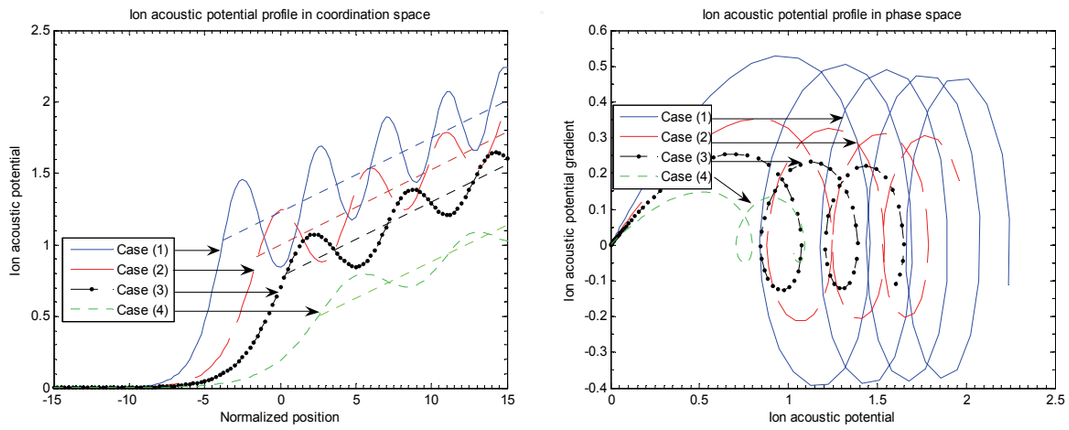

(a) (b)

Fig. 6. Same as Fig. 5 but with $k\lambda_{De} = 1.0\times10^{-1}$ (fixed) for Case (1): $\delta = 1.0\times10^{-5}$, Case (2): $\delta = 2.0\times10^{-5}$, Case (3): $\delta = 3.0\times10^{-5}$, and Case (4): $\delta = 5.0\times10^{-5}$

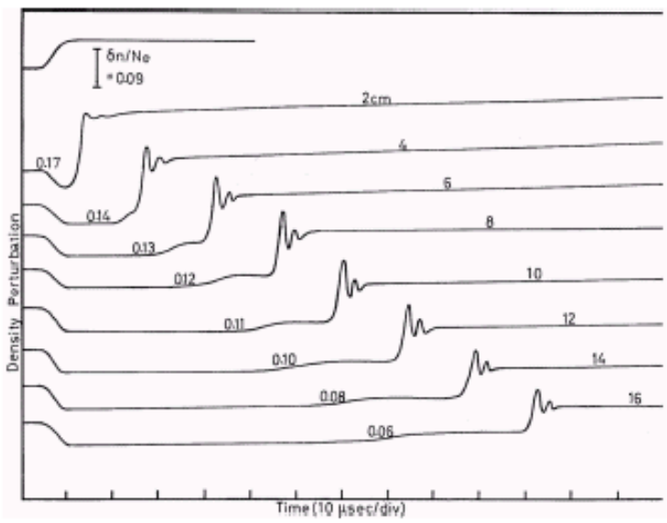

Fig. 7. Experimental profiles of variation of plasma density perturbation (δn) against time (t) at different position of the probe from the grid is shown. Along the *x*-axis, each division represents $10\mu s$ and along the *y*-axis, the density perturbation scale is given as $\delta n/n_e = 0.09$

It is also seen that the value of $\delta = 1 - M_{Dr}$ where resonance occurs remains invariant to spectral variation in source term even by orders of $1.0\times10^{-1} - 1.0\times10^{-10}$. The nonlinear and dispersive coefficients exhibit very sensitive role on even slight variation of δ from its resonance. It is noted that as the value of $\delta = 0$, the usual KdV soliton is recovered, irrespective of any wave number value in the source term. The source term plays an effective role only when finite $k\lambda_{De}$ and δ-values are assigned simultaneously

4.3 Comments

As per experimental observations, oscillatory shocks are reported to emerge from the transonic zone in the target plasma as shown in Fig. 7. One can qualitatively argue that as soon as the solitary wave passes through the unstable transonic zone, it may experience the transient phase modifications leading thereby to the formation of oscillatory shock. The observed damping of the oscillatory shock may be correlated to the non-resonant type of dissipation through phase incoherence among ion acoustic spectral components of the usual solitary wave. It seems to be more plausible to argue that the input energy to the usual soliton due to transonic plasma equilibrium may be shared among different spectral components through adiabatic energy exchange processes. This is concluded here that the complex coefficients of the KdV equation should, in principle, not become the criterion for the non-existence of localized nonlinear solutions including usual solilton, too. But the usual soliton solution exists only for infinitely long wavelength source perturbation. This conclusion is derived subject to the validity condition of our arguments of global temporal phase modification of usual soliton amplitude under unstable condition of the plasma medium. The unstable condition of the medium may cause structural deformation of the non-driven KdV solution. Such deformations may result into sinusoidal (linear) or non-sinusoidal (nonlinear) peaks of oscillatory shock-like solution depending on the wavelength of the source perturbations [8-9, 12].

Applying the wave packet model for a moving soliton leaving behind an acoustic tail of dispersive waves known as precursor or acoustic wind (in soliton frame), the asymmetry can be associated with elevation of the bottom potential by a finite dc value superposed with periodic repetition of linear or nonlinear peaks. The amplification or suppression of a single soliton can be possible only for infinitely long wavelength (dc) source. For shorter wavelength source driving, the transition from usual soliton solution to oscillatory shock-like solutions is more likely to occur. It is, in brief, concluded that the present mathematical study of *d*-KdV equation offers a significant contribution of analytical supports to our numerical prediction of structural transformation of the traveling nonlinear ion acoustic waves in transonic plasma equilibrium of desired quality. It clearly shows that the actual solution of *d*-KdV equation is a resultant of linear mixing (superposition) of soliton and shock both.

Dominating features of the individual nonlinear modes is decided by an appropriate choice of the specific values of unstable wave number (or wavelength) for a given value of the ion flow Mach number. It is obvious to note that in zero growth limit of *d*-KdV equation, the shock-term disappears and only soliton remains. This limit is correlated with dc range of the chosen unstable wave number of quite weaker dispersion strength. As the dispersion strength becomes significant to influence the original soliton strength of weak nonlineariy and weak dispersion in the defined transonic plasma of finite extension, structural modification of the usual KdV soliton profile occurs.

We further argue that the linear and nonlinear normal mode behaviors of the ion acoustic waves in transonic plasma condition differ qualitatively from those derived for static and

dynamic equilibriums without electron inertial correction. The finite but weak hydrodynamic tailoring of the electron fluid motion on ion acoustic space and time scales brings about this difference. It is then argued that the plasma flows in transonic equilibrium should exhibit rich spectrum of linear and nonlinear ion acoustic waves and oscillations. Of course, under Vlasov model the hot electrons with streaming velocity comparable to the phase speed of the ion sound wave may destabilize the ion sound mode through wave-particle resonance effect [8 and references] too. However, our excitation mechanism of ion sound wave differs from the other known mechanisms [8] to excite the same ion sound wave on many grounds [8]. This kind of theoretical scenario of *transonic plasmas* offers a unique scope of *acoustic spectroscopy* to describe the internal state of transonic equilibrium of plasma flows [28].
These calculations have potential applications [26] extensively to understand plasma acoustic dynamics in colloidal plasmas too, but under transonic equilibrium configuration. A generalized statement thereby is reported that all possible sound modes in multi-species colloidal plasmas with drift motions (of inertial ionic species) could be destabilized by the inertial delay effect of the corresponding plasma thermal species that carry out thermal screening of acoustic potential developed due to respective inertial ionic species. Of course, threshold values may differ depending on the choice of the plasma sound mode under consideration. In technological application point of view, one may argue that the proposed theoretical model for inertia-induced acoustic instability mechanism may be utilized to make a plasma-based micro device for *acoustic amplifier* [26]. The amplified acoustic signals (developed due to respective inertial ionic species) from the amplifier could be detected, received and analyzed for the diagnosis and characterization of hydrodynamic flow of plasmas with embedded inertial dust contaminations. These analyses may have potential applications in different ion acoustic wave turbulence-related situations like aerodynamics, solar wind and space plasmas, fusion plasmas, industrial plasmas and plasma flows in astrophysical context, etc.

5. Astrophysical normal acoustics

A plasma-based Gravito-Electorstatic Sheath (GES) model is proposed to discuss the fundamental issues of the solar interior plasma (SIP) and solar wind plasma (SWP). Basic concepts of plasma-wall interaction physics are invoked. Here the wall is defined by a continuous variation of gravity associated with the SIP mass. The neutral gas approximation of the inertially confined SIP is relaxed, and as such the scope of quasi-neutral plasma sheath formation is allowed to arise near the self-consistently defined solar surface boundary (SSB). Analytical and numerical results are obtained to define the SSB and discuss the physics of the surface properties of the Sun, and hence, those of the SWP.

5.1 Physical model description

The SIP system can be idealized as a self-gravitationally bounded quasi-neutral plasma with a spherically symmetric surface boundary of nonrigid and nonphysical nature. The self-gravitational potential barrier of the solar plasma mass distribution acts as an enclosure to confine this quasi-neutral plasma. An estimated typical value ~10^{-20} of the ratio of the solar plasma Debye length and Jeans length of the total solar mass justifies the quasi-neutral behavior of the solar plasma on both the bounded and unbounded scales. Here the zeroth-order boundary surface can be defined by the exact hydrostatic condition of gravito-electrostatic force balancing of the enclosed plasma mass at some arbitrary radial position

from the center of the mean solar gravitational mass. With this much background in mind, let us now formulate the problem of the physical and mathematical descriptions GES formation around the SSB. For simplicity, we consider spherical symmetry of the inertially confined SIP mass, which helps to reduce the three dimensional problem of describing the GES into a simplified one dimensional problem in the radial direction. Thus, only a single radial degree of freedom is required for description of the dynamical behavior of the SWP under the assumed spherically symmetric self-gravitating solar plasma mass distribution.

The idea of the GES formation can be appreciated with quantitative estimates of the gravito-thermal coupling constants for the SIP electrons and hydrogen ions. Henceforth, "ions" and "hydrogen ions" will be used in the sense of the same ionic species. These parameters [10] can be defined and estimated as follows: The gravitothermal coupling constant for electrons can be estimated as $\Gamma_e = k_B T_e / m_e g_\Theta R_\Theta \approx 10$, for a mean electron temperature of $T_e \sim 10^5$ K and as $\Gamma_e \approx 800$ for mean $T_e = 10^6$ K. The notation k_B (=1.3806×10-23 JK-1) denotes the Boltzmann constant**.** Similarly, the gravito-thermal coupling constant for ions can be estimated as $\Gamma_i = (T_i m_e / T_e m_i)\Gamma_e << 1$ for mean $T_e \sim 10^5$ *K*, and $\Gamma_i \approx 1$ for mean $T_e \sim 10^6 K$. Here $g_\Theta = GM_\Theta / R_\Theta^2$ denotes the value of the solar surface gravity. The values of the other constant quantities are taken to be $G = 6.6726 \times 10^{-8}$ dyn cm² g $^{-2}$, $M_\Theta = 1.90 \times 10^{33}$ g, and $R_\Theta = 6.97 \times 10^{10}$ cm.

These estimates are based on the condition of an isothermal SIP, where T_e and T_i respectively denote the electron and ion temperatures. It is now easy to see that the electrons can very well overcome the gravitational potential barrier at the SSB in the standard solar model, whereas the ions cannot. This is the reason why a surface polarization-induced space charge (electrostatic) field is likely to appear, due to thermal leakage of the electrons from the SSB in the radially outward direction. Moreover, the neutral gas approximation for the SIP may not be a good one for describing the properties of the SSB. Similar realizations have already occurred to previous authors [5, 9, 11, 14] for the SWP as well. We take the SIP to be an ideal nonisothermal plasma gas with relatively cold ions. The mean electron temperature $T_e > 10^6$ K for the SIP emerges as a more suitable choice for our theoretical consideration.

According to our GES-model analyses, the GES divides into two scales: one bounded, and the other unbounded. The former includes the steady state equilibrium description of the SIP dynamics bounded by the solar self-gravity. This extends from the solar center to the self-consistently defined and specified SSB. The unbounded scale encompasses the SWP dynamics extending from the SSB to infinity. The SIP electrons can easily escape from the defined SSB. On the other hand, the SIP ions cannot cross the gravitational potential barrier of the solar mass on their thermal energy alone. However, surface leakage of the SIP electrons is bound to produce an electrostatic field by virtue of surface charge polarization. This, in turn, provides an additional source to act on the SIP ions to further energize and encourage them cross over the solar self-gravitational potential barrier.

5.2 Basic governing equations

In order to describe the plasma-based GES physics of our model system, we adopt a collisionless unmagnetized plasma fluid for simplicity in mathematical development to obtain some physical insight into the solar wind physics. The role of magnetic field is also ignored (just for mathematical simplicity) in discussing the collisionless SIP and SWP

dynamics. Applying the spherical capacitor charging model [3], the coulomb charge on the SSB comes out to be $Q_{SSB} \sim 120C$. The mean rotational frequency of the SSB about the centre of the SIP system is is determined to be $f_{SSB} \sim 1.59\times10^{-12}\,Hz$ [42]. Applying the electrical model [42] of the Sun, the mean value of the strength of the solar magnetic field at the SSB in our model analysis is estimated as $\langle|B_{SSB}|\rangle = 4\pi^2 Q_{SSB}\, f_{SSB} \sim 7.53\times10^{-11}\,T$, which is negligibly small for producing any significant effects on the dynamics of the solar plasma particles. Thus the effects of the magnetic field are not realized by the solar plasma particles due to the weak Lorentz force, which is now estimated to be $F_L = e(v\times B) \approx 3.61\times10^{-33}\,N$ corresponding to a subsonic flow speed $v \sim 3.00\,cm\,s^{-1}$ with the input data available [2, 42] with us and hence, neglected. Therefore our unmagnetized plasma approximation is well justified in our model configuration. In addition, the effects of solar rotation, viscosity, non-thermal energy. For further simplification, the electrons are assumed to obey a Maxwellian velocity distribution. Although these approximations may not be realistic, but they may be considered working hypotheses to begin with an ideal situation. Deviations indeed exist from a Maxwellian velocity distribution. We however use it as a working hypothesis for our model considerations. As a result, the usual form of the Boltzmann density distribution for plasma thermal electrons with all usual notations is given as

$$N_e = e^{\theta}. \tag{20}$$

Here $N_e = n_e/n_0$ denotes the normalized electron density. The generic notation $\theta = e\phi/T_e$ denotes the normalized value of the plasma potential associated with the GES on the bounded scale and with the SWP on unbounded scale. The general notation n_e stands for the nonnormalized electron density and $n_0 = \rho_\Theta/m_i$ defines the average bulk density of the equilibrium SIP. The notation $\rho_\Theta = 1.43$ g cm^{-3} stands for the average but constant solar plasma mass density and $m_i = 1.67\times10^{-24}$ g for the ionic (protonic) mass. Again e represents the electronic charge unit and ϕ, the nonnormalized plasma potential associated with both the GES and SWP.

The hydrogen ions are described by their full inertial response dynamics. This includes the ion momentum equation as well as the ion continuity equation. The first describes the change in ion momentum under the action of central gravito-electrostatic fields of potential gradient and forces induced by thermal gas pressure gradients. The latter equation is considered a gas dynamic analog of plasma flowing through a spherical chamber of radially varying surface area. In normalized forms, the ion momentum equation is

$$M\frac{dM}{d\xi} = -\frac{d\theta}{d\xi} - \varepsilon_T \frac{1}{N_i}\frac{dN_i}{d\xi} - \frac{d\eta}{d\xi}. \tag{21}$$

Here the minus sign in the gravitational potential term indicates the radially inward direction of the solar self-gravity. The deviation from the conventional neutral gas treatment of the SIP is introduced through the electric space charge-induced force (first term on right-hand side) effect. The normalized expression for conservation of ion flux density is

$$\frac{1}{N_i}\frac{dN_i}{d\xi} + \frac{1}{M}\frac{dM}{d\xi} + \frac{2}{\xi} = 0. \tag{22}$$

The normalizations are defined as follows:

$$\theta = \frac{e\phi}{T_e},\ \ \eta = \frac{\psi}{C_s^2},\ \ N_e = \frac{n_e}{n_0},\ \ N_i = \frac{n_i}{n_0},$$

$$M = \frac{v_i}{c_s},\ \ \xi = \frac{r}{\lambda_J},\ \ \lambda_J = \frac{c_s}{\omega_J},\ \ c_s = \left(\frac{T_e}{m_i}\right)^{1/2},$$

$$\omega_J = \left(4\pi\rho_\Theta G\right)^{1/2},\ \ \varepsilon_T = \frac{T_i}{T_e}.$$

The notations ϕ and ψ respectively stand for the dimensional (*unnormalized*) values of the plasma electrostatic potential and the self-solar gravitational potential as variables associated with the GES. The dimensional values of the electron and ion population density variables are respectively denoted by n_e and n_i. Likewise, the dimensional ion fluid velocity variable is represented by the symbol v_i. The notation η stands for the normalized variable of the self-solar gravitation potential. The notation N_i denotes the normalized value of the ion particle population density variable. Notation M stands for the ion flow Mach number.

The notations r and ξ stand for the nonnormalized and normalized radial distance respectively from the heliocenter in spherical co-ordinates. The other notations λ_J, c_s and ω_J defined as above stand for the Jeans length, sound speed and Jeans frequency respectively. Finally, the notation ε_T as defined above stands for the ratio of ion to electron temperature. The ion flux density conservation (eq. 22) contains a term that includes the effect of geometry on the ion flow dynamics of the SIP mass, self-gravitationally confined in a spherical region, whose size is to be determined from our own model calculations. Equations (21) and (22) can be combined to yield a single expression representing the well-known steady state hydrodynamic flow,

$$\left(M^2 - \varepsilon_T\right)\frac{1}{M}\frac{dM}{d\xi} = -\frac{d\theta}{d\xi} + \varepsilon_T\frac{2}{\xi} - \frac{d\eta}{d\xi}. \tag{23}$$

There is an obvious difference in the above equation from the corresponding momentum equation under the neutral gas approximation for the SIP. The difference appears, as discussed above, in the form of a space charge effect originating from the Coulomb force on a collective scale (first term on the right-hand side of eq. (21)).

The gravito-electrostatic Poisson equations complement the steady dynamical equation (23) for a complete description of the gravito-electrostatic sheath structure, which is formed inside the non-rigid SSB. This is important to emphasize that in the case of a real physical boundary, the plasma sheath is always formed both inside and outside the boundary surface in its close vicinity [12]. The normalized forms of the gravitational and electrostatic Poisson equations for the SWP description are respectively given by

$$\frac{d^2\eta}{d\xi^2} + \frac{2}{\xi}\frac{d\eta}{d\xi} = N_i\text{, and} \tag{24}$$

$$\left(\frac{\lambda_{De}}{\lambda_J}\right)^2\left[\frac{d^2\theta}{d\xi^2}+\frac{2}{\xi}\frac{d\theta}{d\xi}\right]=N_e-N_i\,. \tag{25}$$

Here $\lambda_{De}=\left(T_e/4\pi n_0 e^2\right)^{1/2}$ denotes the plasma electron Debye length of the defined SIP system. The other quantities are as defined above as usual. Equations (21)–(25) constitute a completely closed set of basic governing equations with which to discuss the basic physics of the GES-potential distribution on the bounded scale. Of course, the discussion also includes the associated ambipolar radial flow variation of the SIP towards an unknown SSB which we have to determine self-consistently in this problem with GES-based theory. For a typical value $T_e=10^6$ K, one can estimate that $\lambda_{De}/\lambda_J\approx 10^{-20}$ which implies that the Debye length is quite a bit smaller than the Jeans scale length of the solar plasma mass. Thus, on the typical gravitational scale length of the inertially bounded plasma, the limit $\lambda_{De}/\lambda_J\to 0$ represents a realistic (physical) approximation. By virtue of this limiting condition, the entire SIP extending up to the solar boundary and beyond obeys the plasma approximation. Thus, the quasi-neutrality condition as given below holds good

$$N_e=N_i=N=e^{\theta}. \tag{26}$$

This is to note that equation (26) does not mean that the plasma ions are Boltzmannian in thermal character, but inertial species. Equation (26) can be differentiated once in space and further rewritten as,

$$\frac{1}{N}\frac{dN}{d\xi}=\frac{d\theta}{d\xi}. \tag{27}$$

By virtue of the plasma approximation, one can justify that the GES of the SIP origin should behave as a quasi-neutral space charge sheath on the Jeans scale size order. The formation mechanism of the defined GES, however, is the same as in the case of plasma-wall interaction process in laboratory confined plasmas. From equations (26)-(27), it is clear that for the electrostatic potential and its gradient being negative, causes the exponential decrease of the plasma density. Finally, the reduced form of the basic set of autonomous closed system of coupled nonlinear dynamical evolution equations under quasi-neutral plasma approximation is enlisted as follows

$$\left(M^2-\varepsilon_T\right)\frac{1}{M}\frac{dM}{d\xi}=-\frac{d\theta}{d\xi}+\varepsilon_T\frac{2}{\xi}-\frac{d\eta}{d\xi}, \tag{28}$$

$$\frac{d\theta}{d\xi}+\frac{1}{M}\frac{dM}{d\xi}+\frac{2}{\xi}=0, \text{ and} \tag{29}$$

$$\frac{d^2\eta}{d\xi^2}+\frac{2}{\xi}\frac{d\eta}{d\xi}=e^{\theta}. \tag{30}$$

This set of differential evolution equations constitutes a closed dynamical system of governing hydrodynamic equations that will be used to determine the existence of a bounded GES structure on the order of the Jeans scale length $\left(\lambda_J\right)$ in our GES-model of the

subsonic origin of the SWP of current interest. Thus the solar parameters $M(\xi)$, $g_s(\xi)$ and $\theta(\xi)$ representing the equilibrium Mach number, solar self-gravity and electrostatic potential, respectively, will characterize the gravito-electrostatic acoustics in our approach.

5.3 Theoretical analysis of solar surface boundary

5.3.1 Analytical calculations

We first wish to specify the overall condition for the existence of the SSB. Such existence demands the possibility of a self-consistent bounded solution for the solar self-gravity. The boundary will correspond to a maximum value of the solar self-gravity at some radial distance from the heliocenter. This defines a self-consistent location of the SSB. Before we proceed further, let us argue that the radially outward pulling bulk force effect of the GES-associated potential term in equation (28) demands a negative electrostatic potential gradient, that is, $d\theta/d\xi<0$. This makes some physical sense because the ion fluid has to overcome the gravitational barrier to create a global-scale flow of the SIP in a quasi-hydrostatic way.

Now, if we invoke the concept of exact hydrostatic formation under gravito-electrostatic force balancing $(d\theta/d\xi \approx d\eta/d\xi)$, the surface potential can be solved to get $\theta-\theta_\Theta \approx \eta-\eta_\Theta$. Here the unknown boundary values of $\theta=\theta_\Theta$, $\eta=\eta_\Theta$ and $M=M_{SSB}$ are to be self-consistently specified numerically. The notation (M_{SSB}) stands for the Mach value associated with the SIP flow at the SSB. Now, by the exact hydrostatic equilibrium condition in the set of equations (28)-(30), one can get the following set of equations for the SSB description:

$$\left(M^2-\varepsilon_T\right)\frac{1}{M}\frac{dM}{d\xi}=\varepsilon_T\frac{2}{\xi}, \tag{31}$$

$$-\frac{d\eta}{d\xi}+\frac{1}{M}\frac{dM}{d\xi}+\frac{2}{\xi}=0 \text{ , and} \tag{32}$$

$$\frac{d^2\eta}{d\xi^2}+\frac{2}{\xi}\frac{d\eta}{d\xi}=e^{\theta}. \tag{33}$$

For purpose of the GES analysis, we define the solar self-gravitational acceleration as $g_s=d\eta/d\xi$. Equation (34) thus reads

$$\frac{dg_s}{d\xi}+\frac{2}{\xi}g_s=e^{\theta}. \tag{34}$$

Finally, the SIP and hence, the SSB are described and specified in terms of the relevant solar plasma parameters $M(\xi)$, $g_s(\xi)$ and $\theta(\xi)$ representing respectively the equilibrium Mach number, solar self-gravity and electrostatic potential as a coupled dynamical system of the closed set of equations recast as the following

Solar self-gravity equation:

$$\frac{dg_s}{d\xi}+\frac{2}{\xi}g_s=e^{\theta}, \tag{34a}$$

Ion continuity equation:

$$\frac{d\theta}{d\xi}+\frac{1}{M}\frac{dM}{d\xi}+\frac{2}{\xi}=0, \text{ and} \tag{34b}$$

Ion momentum equation:

$$\left(M^2-\alpha\right)\frac{1}{M}\frac{dM}{d\xi}=\alpha\frac{2}{\xi}-g_s, \tag{34c}$$

where $\alpha=1+\in_T=1+\left(T_i/T_e\right)$, T_e is the electron temperature and T_i is the inertial ion temperature for the bounded solar plasma on the SIP-scale as already mentioned.

Let us now denote the maximum value $\left(g_\Theta\right)$ of solar gravity at some radial position $\xi=\xi_\Theta$ where $\theta=\theta_\Theta$ and apply the necessary condition for the maximization of g_s at a spatial coordinate $\xi=\xi_\Theta$. This condition $\left(dg_s/d\xi\right)_{\xi=\xi_\Theta}=0$ when used in equation (34) yields $\xi_\Theta=2g_\Theta e^{-\theta_\Theta}$. However, it is not sufficient to justify the occurrence of the maximum value of g_s until and unless the second derivative of g_s is shown to have negative value. To derive the sufficient condition for the maximum value of g_s at $\xi=\xi_\Theta$, let us once spatially differentiate equation (34) to yield

$$\frac{d^2g_s}{d\xi^2}-\frac{2}{\xi^2}g_s+\frac{2}{\xi}\frac{dg_s}{d\xi}=e^\theta\frac{d\theta}{d\xi}. \tag{35}$$

Now the condition for the maximization of g_s at the location $\xi=\xi_\Theta$ can be discussed by considering $d\theta/d\xi<0$ in equation (35) under the exact hydrostatic equilibrium approximation $\left(\left|d\theta/d\xi\right|\approx\left|d\eta/d\xi\right|=g_\Theta\right)$ near the solar surface to yield the following inequality

$$\left.\frac{d^2g_s}{d\xi^2}\right|_{\xi=\xi_\Theta}=\frac{2}{\xi_\Theta^2}g_\Theta-e^{\theta_\Theta}g_\Theta=g_\Theta\left(\frac{2}{\xi_\Theta^2}-e^{\theta_\Theta}\right)<0. \tag{36}$$

From these analytical arguments one can infer that the maximization of g_s indeed occurs at some arbitrary radial position that satisfies the inequality: $\xi_\Theta>\sqrt{2}e^{-\theta_\Theta/2}(=2.33)$ for $\theta_\Theta\sim-1$ (Figs. 8b, 9b, and 10b). Numerically the location of the SSB is found to lie at $\xi_\Theta\sim3.5$ that matches with $\xi_\Theta=2g_\Theta e^{-\theta_\Theta}$ for $\theta_\Theta=1.07$ and $g_\Theta=0.6$. It satisfies the analytically derived inequality (36) too. Now the other two equations (32)-(33) can be simultaneously satisfied in the SSB only for a subsonic solar plasma ion flow speed if Mach number gradient acquires some appropriate negative minimum near zero $\left(M\sim\left|\left(dM/d\xi\right)\right|\sim10^{-6}\right)$.

It is indeed seen numerically that near the maximum solar self-gravity of the SIP mass, the first and third terms in equation (32) are almost equal and hence the Mach number gradient term, which is negative in the close vicinity of the SSB, should be smaller than the other two terms so as to satisfy equations (31) and (32), simultaneously. Actually, the three equations (31)-(32) and (34) are solved numerically to describe the SSB of the maximum self-gravitational potential barrier properly where g_s associated with the self SIP mass is maximized.

5.3.2 Numerical calculations

Determination of the autonomous set of the initial values of the defined physical variables is a prerequisite to solve the nonlinear dynamical evolution equations (34a)-(34c) in general as an initial value problem. The initial values of the physical variables like $M(\xi), g_s(\xi)$ and $\theta(\xi)$ are defined inside the solar interior and are determined on the basis of extreme condition of the *nonlinear stability analysis* [4]. The self-consistent choice of the initial values is obtained by putting $dM/d\xi|_{\xi_i} = -e^{\theta_i/2}$, $dg_s/d\xi|_{\xi_i} = 0$ and $d\theta/d\xi|_{\xi_i} = 0$ in these three equations (34a)-(34c). But the realistic SWP model demands that $d\theta/d\xi|_{\xi_i} \neq 0$. Finally, we determine the expressions for a physically valid set of the initial values of the given physical variables as follows,

$$M_i = \frac{1}{2}\xi_i e^{\theta_i/2} \tag{37}$$

$$g_{si} = \frac{1}{2}\xi_i e^{\theta_i} \tag{38}$$

This is to note that the initial values of θ_i and ξ_i are chosen arbitrarily. As discussed later, we find that the SSB acquires a negative potential bias ($\theta_s \sim -1$) of about -1 kV. It also acquires the maximum value of solar interior gravity ($g_\Theta \sim 0.6$) and minimum value of non-zero SIP flow speed ($M_{SSB} \sim 10^{-7}$) at the SSB. The value of the electrostatic potential gradient at the surface comes out to be ~ –0.6. This means that the strength of the GES-associated solar surface gravity and electrostatic potential gradient is almost equal. As a result the SSB is defined by some constant values of the physical variables (g_s, θ, M). The SSB values of these parameters are determined through spatial evolution of the coupled system of equations (34a)-(34c) from the given initial values (37)-(38) inside the SIP zone.

We have used the well-known fourth-order Runge-Kutta method (RK 4) for numerical solutions of equations (34a)-(34c). By numerical analysis (Figs 8-11), we find that the solar radius is equal to thrice of the Jeans length (λ_J) for mean solar mass density $(\rho_\Theta = 1.41 g.cm^{-3})$. From this observation one can easily estimate that $\lambda_j = R_\Theta / 3.5$. Now comparing our own theoretical value of the solar mass self-gravity with that of the standard value, we arrive at the following relationship between the solar plasma sound speed (c_s) and the Jeans length (λ_J)

$$0.6\left(c_s^2/\lambda_J\right) = 2.74\times10^4 \ cm/sec^2. \tag{39}$$

By substituting the value of the Jeans length expressed in terms of the solar radius, one can determine and specify the mean value of the electron temperature, which is $T_e \sim 10^7$ K. The sound speed in the SIP under the cold ion model approximation is thus obtained as $c_s \sim 3\times10^7$ cm s^{-1}. Note that the SWP speed at 1 AU is fixed by the sound speed of the SWP medium, which is determined and specified by the requirement that a transonic transition solution occurs on the unbounded scale of the SWP dynamics description.

The gravito-acoustic coupling coefficient could be estimated as $\Gamma_{g-a} = m_i g_\Theta R_\Theta / T_e \sim 2.0$. In absence of the gravitational force, the bulk SIP ion fluid will acquire the flow speed corresponding to $M \sim 1.41$ for a negative potential drop of the order of $(-T_e/e)$ over a

distance equal to that of the solar radius. If one estimates the value of gravito-acoustic coupling coefficient at this velocity defined by $M \sim 1.41$, it comes out to be unity. Thus the quasi-hydrostatic type of equilibrium gravitational surface confinement of the SIP is ensured. The GES-potential induced outward flow of the SIP is also ensured. Due to comparable strength of the solar surface gravitational effect of deceleration, the net SIP ion fluid flow is highly suppressed to some minimum value (~1.0-3.0 *cm/sec*) corresponding to $M \sim 10^{-7}$ at the SSB.

An interesting point to note here is that near the defined SSB, the electrostatic potential gradient terminates into an almost linear type of profile. The value of its gradient value will provide an estimate of the second order derivative's contribution into the electrostatic potential which measures the level of local charge imbalance near the solar surface. From our computational plots (Figs. 8b, 9b and 10b), this local charge imbalance comes out to be of the order –0.17, which is equivalent to 17% ion excess charge distributed over a region of size on the order of the plasma Debye sheath scale length. However, the same level of the electrostatic local charge imbalance on the Jeans scale length does not require the inclusion of the role of the Poisson term for the evolution of the electrostatic potential's profile under the GES-model. Hence, in this sense the GES is practically equivalent to a quasi-neutral plasma sheath with its potential profile tailored and shaped by the potential barrier of the self-gravity of the SIP mass distribution.

5.3.3 Properties of solar surface boundary

Table I lists the defined initial values of the physical variables (g_s, θ, M) as already discussed and their corresponding boundary values numerically obtained for the description of the desired SSB. The initial values of g_s, θ, and M are associated with the normalized mean SIP mass density, enclosed within a tiny spherical globule having normalized radius equal to an arbitrarily chosen value of ξ_i.

Parameter	At the Initial Radial Point (ξ_i)	At the Solar Surface Boundary (ξ_Θ)	Initial Values
Potential θ	$\frac{d\theta}{d\xi} = 0$	$\frac{d\theta}{d\xi} \sim -0.62$, $\theta_\Theta \sim -1.00$	θ_i, arbitrarily chosen
Gravity g_s	$\frac{dg_s}{d\xi} = 0$	$\frac{dg_s}{d\xi} = 0$, $g_\Theta \sim 0.60$	$g_{si} = \frac{1}{2}\xi_i e^{\theta_i}$, derived
Mach number M	$\frac{dM}{d\xi} = -e^{\theta_i/2}$	$\frac{dM}{d\xi} = 0$, $M_{SWP} \sim 10^{-7}$	$M_i = \frac{1}{2}\xi_i e^{\theta_i/2}$, derived

Table 1. Initial and Boundary Values of Relevant Solar Parameters

From the numerical plots shown in Figs. 8-10, we find that the minimum Mach number (M_{SSB}) at the specifically defined SSB comes out to be of order 10^{-7}. For this value of Mach number, equation (31) can be simplified to show that near the boundary, $dM/d\xi \approx -M/\xi_\Theta = -3\times10^{-8} \sim 0$. This corresponds to a quasi-hydrostatic type of the SSB equilibrium. It arises from gravito-electrostatic balancing with an outward flow of the SIP having a minimum speed of about 1-3 cm s^{-1}. With these inferences one can argue that the

SWP originates by virtue of the interaction of the SIP with the SSB. Hence an interconnection between the Sun and the SWP can be observed by applying the GES model. Here the boundary is not sharp but distributed over the entire region of the solar interior volume. The basic principles of the GES coupling govern the solar surface emission process of the subsonic SWP.

As depicted in table I, the time-independent solar g_s-profile associated with the SIP mass distribution terminates into a diffuse surface boundary. This is characterized and defined by the quasi-hydrostatic equilibrium $g_s = g_\Theta \sim |d\theta/d\xi|$, which occurs at about $\xi = \xi_\Theta \sim 3.5$ (see Figs. 8-10). As such, the basic physics of the subsonic origin of the SWP from the SSB is correlated with the bulk SIP dynamics. We note that the precise definition of the SSB influences the SWP velocity at 1 AU. Other models report similar observations too [3, 31-41]. The dependence on the ion to electron temperature ratio is quite visible in Fig. 11a. Let us now discuss the numerical results in the figures individually.

Figure 8 depicts the time-independent profiles of (g_s, θ, M) and their variations with the ion-to-electron temperature ratio ε_t for fixed values of the initial point ($\xi_i = 0.01$) and plasma sheath potential ($\theta_i = -0.001$). As shown in Fig. 8a, the location of the SSB remains the same but its maximum value changes, and a most suitable choice of ε_t = 0.4 is identified for which the quasi-hydrostatic condition is fulfilled. The *E*-field profile is invariant for all chosen values ε_t =0-0.5. Again, as shown in Fig. 8b, the electrostatic potential corresponding to $\varepsilon_t \sim$ 0.4 comes out to be $\theta = \theta_\Theta \sim -1$ (i.e. ~1 kV). Similarly, Fig. 8c depicts the minimum Mach value of $M_{SSB} \sim 10^{-7}$ for ε_t ~0.4 varying by a factor of 2 for other values of ε_t.

Figure 9 depicts the time-independent profiles of g_s, θ, and M and their variations with initial position for fixed values of ε_t =0-0.4 and $\theta_i = -0.001$. It can be seen that the most suitable choice of the initial position for our fixed values θ_i and ε_T comes out to be $\xi_i \sim 0.01$, which is consistent with the earlier value shown in Fig. 8a. Moreover, the minimum value of *M*~10^{-7} (Fig. 9c) is also consistent with the earlier value shown in Fig. 8c.

Figure 10 depicts the time-independent profiles of g_s, θ, and M and their variations with electrostatic potential for fixed values of $\xi_i = 0.01$ and $\varepsilon_T = 0.4$. It is observed fascinatingly that the most suitable choice of the initial value of the normalized electrostatic potential for our fixed values of ξ_i and ε_T comes out to be $\theta_i = -0.001$.

It is notable that high initial drop of *M*-profile occurs as shown in Fig.8c, Fig. 9c and Fig. 10c. This indicates the over dominance of the solar interior gravity up to about $\xi \sim 1.5$, and thereafter, the *E*-field becomes comparable, balancing at about $\xi \sim 3.5$. Thus the normalized width of the *gravito-electrostatic sheath* could be estimated and denoted by $\xi_{G-E} \sim 2$. This is a quasi-neutral space charge region with positive charge (ion) excess near the defined SSB wall. Thus a self-consistent bounded solution of nonlinearly coupled gravito-electrostatic potential profiles exists. It forms a quasi-hydrostatic equilibrium at the SSB for the choice of the appropriate set of the initial parameter values $\theta_i = -0.001$ & $\xi_i = 0.01$ for $\varepsilon_T = 0.4$. This is not a rigid boundary at all. As a result the SSB is capable to exhibit many kinds of global oscillation dynamics governed by the nonlinear coupling of the gravito-electrostatic sheath potentials.

For a laboratory hydrogen plasma, the normalized floating potential can be estimated as $\theta_f = -3.76$ under the flat surface approximation. Now, if we consider the numerically calculated minimum value of *M* for our solar surface characterization, the estimated value of

θ_f is about -20 using the flat surface approximation. This is a crude estimate because the solar surface potential drop occurs over a distance of the order of the Jeans scale where the effect of curvature should not be ignored. The numerically obtained solar surface potential is quite a bit smaller than the floating potential. Simply put, this means that the defined SSB of the GES-model draws a finite amount of electron-dominated electric current that flows toward the heliocenter.

Let us invoke a generalized concept of the plasma sheath, which is traditionally associated with a localized electrostatic potential only in the plasma physics community. We argue that any localized nonneutral space charge layer (in our case, on the order of the Jeans length) is the result of a self-consistent nonlinear coupling of gravito-electrostatic force field variations. This is what we mean by the GES, which of course, obeys the global quasi-neutrality condition because of the smallness of the ratio λ_{De}/λ_J for the SIP parameters.

5.4 Acceleration of solar interior plasma

5.4.1 Basic equations for SWP descriptions

We have already argued that the subsonic origin of the SWP from the SSB is an outcome of the condition of quasi-hydrostatic equilibrium at the boundary. This is a result of the comparable, but competiting strengths of the gravitational deceleration and the electrostatic acceleration of the SIP near the SSB. Now we will try to look at the problem of solar wind acceleration from subsonic to supersonic speed. This is referred to as the *transonic transition* behavior of the outward-moving SIP in the form of the SWP. Let us now argue that the radial variation of Mach number and electrostatic potential beyond the defined SSB should be described by the following autonomous set of coupled nonlinear differential equations

$$\left(M^2-\varepsilon_T\right)\frac{1}{M}\frac{dM}{d\xi}=-\frac{d\theta}{d\xi}+\varepsilon_T\frac{2}{\xi}-\frac{1}{\xi^2}\frac{GM_\Theta}{C_s^2\lambda_J}\text{, and} \tag{40}$$

$$\frac{d\theta}{d\xi}+\frac{1}{M}\frac{dM}{d\xi}+\frac{2}{\xi}=0\,. \tag{41}$$

Let us note that the constant SIP mass acts as an external object to offer a source of gravity for tailoring and monitoring the outgoing SIP flow with the initially subsonic speed specified at the defined SSB. The Poisson equation for gravity is now redundant. It is important to comment that the electrostatic force field is not imposed from outside to control the solar wind's motion. In fact, the required electric field for the SWP acceleration is of internal origin. Equations (40) and (41) can be combined to yield a single coupled form as given below

$$\left[M^2-\left(1+\varepsilon_T\right)\right]\frac{1}{M}\frac{dM}{d\xi}=\left(1+\varepsilon_T\right)\frac{2}{\xi}-\frac{1}{\xi^2}\frac{GM_\Theta}{C_s^2\lambda_J}. \tag{42}$$

The quantity $a_0=GM_\Theta/c_s^2\lambda_J$ (*normalization coefficient*) is treated as a free parameter, which eventually provides a way to estimate the SWP electron temperature. The value of this parameter is determined by the condition that a transonic solution for the SWP exists for a given set of initial values of the required physical variables. The above equation can now be rewritten as

$$\left[M^2-(1+\varepsilon_T)\right]\frac{1}{M}\frac{dM}{d\xi}=(1+\varepsilon_T)\frac{2}{\xi}-\frac{a_0}{\xi^2}. \quad (43)$$

5.4.2 Numerical results

Equations (41) and (43) can be solved by numerical methods (by Runge-Kutta IV method) to determine the time independent $M-$ and $\theta-$ profiles associated with the SWP for some arbitrary values of a_0. However, we choose the minimum value of a_0 that yields transonic transition solutions. It is obvious from equation (43) that the critical distance will exist at $\xi=\xi_c=a_0/2(1+\varepsilon_T)$. This critical distance corresponds to $\sim 14R_\Theta$ from the defined solar surface. As shown in Fig. 10, the critical point for transonic transition, indeed, exists for a_0 = 95 for narrow range variation of $\varepsilon_T=0.0-0.1$, for the already derived solar surface values of $M_{SSB}=10^{-7}$ & $\theta_\Theta=-1.0$ as a set of initial values. The M-values at a distance of 1AU from the defined SSB, i.e., at $\xi\sim 750$ are about 3.3 and 3.5 for $\varepsilon_T=0.0$ & 0.1, respectively, as shown in Fig. 11a. The corresponding values of the electrostatic potential at the same distance are found to be $\theta=-31$ & -30 for $\varepsilon_T=0.0$ & 0.1, respectively as shown in Fig. 11b. This is to note that for higher values of ε_T, solar breeze solutions are obtained.

Substitution of $\lambda_J=R_\Theta/3.5$ in the defined expression of a_0 = 95, we can estimate c_s ~100 *km/sec* and T_e ~100 *eV* for the SWP. The critical distance for transition behavior to occur for M_{SSB} ~10^{-7} (Fig. 11a) as an initial value for Mach number exists at about $14R_\Theta$ distance apart from the defined solar surface. This is to note that if we consider M_{SSB} ~10^{-6} as an initial value for the numerical solution of equations (41) and (43), the transonic transition occurs for a_0 = 71 that yields almost the same values of c_s ~100 *km/sec* and T_e ~100 *eV* for the SWP. But the critical transition location point exists at about $10R_\Theta$ distance apart from the defined solar surface. This implies the initial value of M_{SSB} plays an important role in the proper fixation of a_0 that determines the exact location of transonic transition point and the SWP-property. Accordingly, the speed of the SWP at 1 AU comes out to be 330-350 km s^{-1}, as shown in Fig. 11a (dotted vertical line).

Let us now look at Fig. 11b which the electrostatic potential's profile for a predetermined set of initial values of $M_{SSB}=10^{-7}$, and $\theta_\Theta\sim -1$ at the SSB, as in the case of Fig. 11a. It can be seen that the normalized value of the SWP-associated electrostatic potential at 1 AU is about -30 to -31 for $\varepsilon_T=0.0-0.1$. With some simple calculations, as illustrated in the next subsection, we can argue that beyond the transonic transition, the SWP seems to obey the zero-electric current approximation, but not before. This is inferred from the floating surface condition, which is defined by the equalization of escaping flux of the SWP particles in accordance with the law of conservation of particle flux.

5.4.3 Theoretical estimation of floating potential

In absence of any particle source and/or sink of a stellar origin under spherical geometry approximation, we get an expression for the steady state mass conservation of the SWP flow

$$r^2 n_{iT} v_i = r_{SSB}^2 n_0 v_{SSB}. \quad (44)$$

In normalized form the above expression (44) for N_i=n_i/n_0=1, can be written as

$$M = \left(\xi_{SSB}^2 / \xi^2\right) M_{SSB}. \tag{45}$$

Now using normal practice for floating potential estimation under net zero-electric current approximation, i.e. $J_e = J_i$,, one gets

$$e^{\theta_f} \sqrt{\left(m_i / m_e\right)} = M = \left(\xi_{SSB}^2 / \xi^2\right) M_{SSB}. \tag{46}$$

Now, from equation (47) the normalized floating potential at any normalized radial position from the SSB can be expressed as

$$\theta_f = \log\left[\sqrt{\frac{m_e}{m_i}} \left(\frac{\xi_{SSB}}{\xi}\right)^2 M_{SSB}\right]. \tag{47}$$

By simple calculations, one can generate the following comparative data of theoretical estimation of the SWP floating potential (using above expression (47)) at different distances from the obtained SSB as follows.

ξ	θ_f
3.50 (at ξ_Θ)	-19.57
47.50 (at ξ_c)	-24.78
100	-26.27
200	-27.66
300	-28.47
400	-29.04
500	-29.49
600	-29.86
700	-30.16
750 (1 AU)	-30.30

Table 2. Values of the Floating Potential

It looks as if the SSB was in non-floating condition as because it does not acquire floating potential during evolution of the GES-potential distribution of the SIP. However, beyond the critical distance and up to a distance of 1 *AU*, the calculated values of the floating potential almost match with those of the SWP obtained numerically (Fig. 11b). This implies that a finite divergence-free electric current exists at the SSB up to the transonic transition region! Beyond the transonic point, zero electric current approximation seems to hold good.

It is commented that the zero-electric current approximation at the SSB assumed in previous model calculations [3, 11, 31-41] for the qualitative description of the SWP properties seems to be physically unjustified. Furthermore, our model calculation does not require outside imposition of the electric field to ensure the validity of the zero-electric current approximation at the SSB. Probably the imposition of the zero-electric current approximation is not suitable for proper description of the SWP properties. Now the natural question may arise, "What happens to the SWP current after the transonic transition?" It

seems the current dissipates mainly through a channel of inertial resistance of the plasma ions due to solar gravity.

5.5 Physical consequences

5.5.1 Description of numerical results

The proposed GES-model predicts that the GES formation (of the SIP origin) drives the subsonic SWP at the solar surface. The quasi-hydrostatic equilibrium defines the solar boundary and ensures the GES formation. Numerically $\theta_\Theta \sim -1$, M_{SSB} ~10^{-7}, and $g_\Theta \approx |d\theta/d\xi| \sim 0.60$ prescribe the defined solar boundary (Table I). It requires specific initial values $\theta_i = -0.001$ & $\xi_i = 0.01$ in the solar interior for $\varepsilon_T = 0.4$.

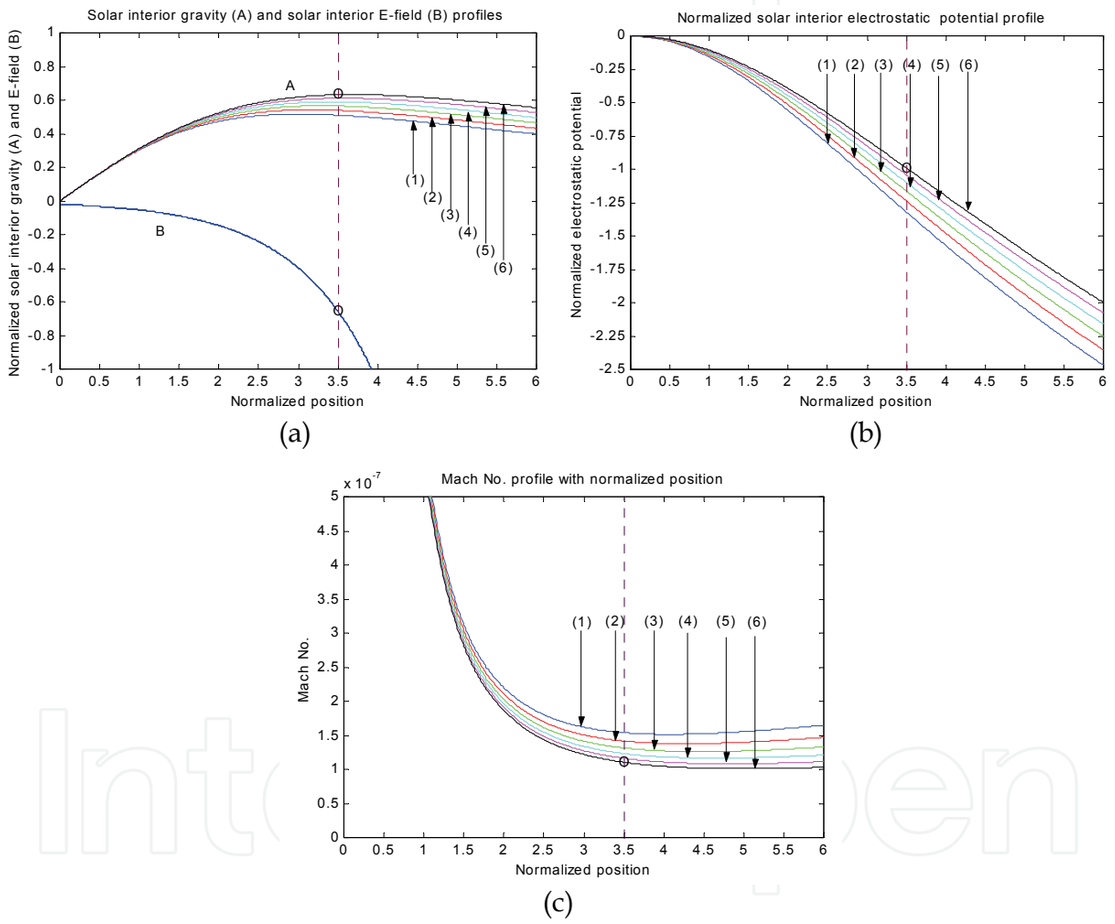

Fig. 8. Variation of normalized values of (a) solar interior gravity $d\eta/d\xi$ (upper group of curves) and electric field $d\theta/d\xi$ (lower curve), (b) electrostatic potential θ, and (c) speed M associated with solar interior plasma flow dynamics with normalized position (ξ) from the heliocenter $(\xi = 0)$. The values of initial position $\xi_i = 0.01$ and initial electrostatic potential $\theta_i = -0.001$ are held fixed. The lines correspond to the cases ε_T = 0.0 (graph 1), 0.1 (graph 2), 0.2 (graph 3), 0.3 (graph 4), 0.4 (graph 5), and 0.5 (graph 6) respectively. The defined solar surface boundary lies at a radial position $\xi_\Theta \sim 3.5$ (implying $R_\Theta \sim 3.5\lambda_J$) with circled points corresponding to the solar surface values

Item	Parker's model	GES Model
1.	Deals with an unbounded solution of steady state hydrodynamic equilibrium of the solar wind (SW)	Deals with bounded (SIP) and unbounded (SWP) solutions of a continuum steady state hydrodynamic equilibrium
2.	Considers a single neutral fluid (gas) model approximation for the SW gas flow dynamics	Considers a two-fluid ideal plasma (gas) model for the SIP and SWP gas flow
3.	Predicts an unbounded solution of supersonic expansion of the SW provided that a sub-sonic flow pre-exists at the SSB	Predicts a bounded solution of the SIP mass distribution with its subsonic outflow at the SSB
4.	Genesis of the subsonic solar surface origin of the SW is not precisely known: discusses the acceleration of the SW by analogy with the de Laval nozzle	Discusses the genesis of the subsonic SSB origin of the SIP in terms of the basic principles of the GES acceleration of ions: the transonic acceleration mechanism of the SWP is the same as Parker's
5.	Does not specify precisely the SW-base definition and prescription for the self-consistent SSB	Offers a precise definition of and prescription for a self-consistent SSB
6.	Standard solar surface is electrically uncharged and unbiased	SSB acquires a negative electrostatic potential (~1 kV) at the cost of thermal loss of the electrons
7.	Does not consider plasma-boundary wall interaction, plasma sheath formation and spontaneous thermal leakage through squeezing mechanism	Considers it
8.	Concept of floating surface (at which no net electric current) is not involved	It is involved
9.	Considers one-scale (SW) theoretical description	Considers two-scale (SIP and SWP) theoretical description
10.	Extensive research has already been done on the SW acceleration and heating	Opens a new chapter of the GES-based theory for interior (bounded) and exterior (unbounded) solar plasma flow dynamics

Table 3. Parker versus GES Model

The GES-formation occurs due to solar surface leakage of the thermal electrons of solar interior plasma outgoing radially outwards. It causes an appreciable space charge polarization effect near the boundary. The depth of the electrostatic potential well for the plasma ions, so formed, is such as to allow the incoming ions from the solar interior bulk plasma to acquire the kinetic energy of ion motion to overcome the maximum gravitational potential barrier height near the boundary. The SIP ions come out of the solar gravitational barrier with a minimum speed M_{SSB} ~10^{-7}. From the floating potential calculation with no net current flow, we infer that the solar surface boundary drives out some finite electric current in the outward flow. That is, it seems a finite electric current loss of the SIP occurs through its leakage process near the SSB! It can be shown that the total surface charge in the boundary, however, comes out to be about 10^{20} times the electronic charge. Table III gives a glimpse of distinction between Parker's model and GES-model of the subsonic SWP origin and its acceleration from subsonic to supersonic flow speed.

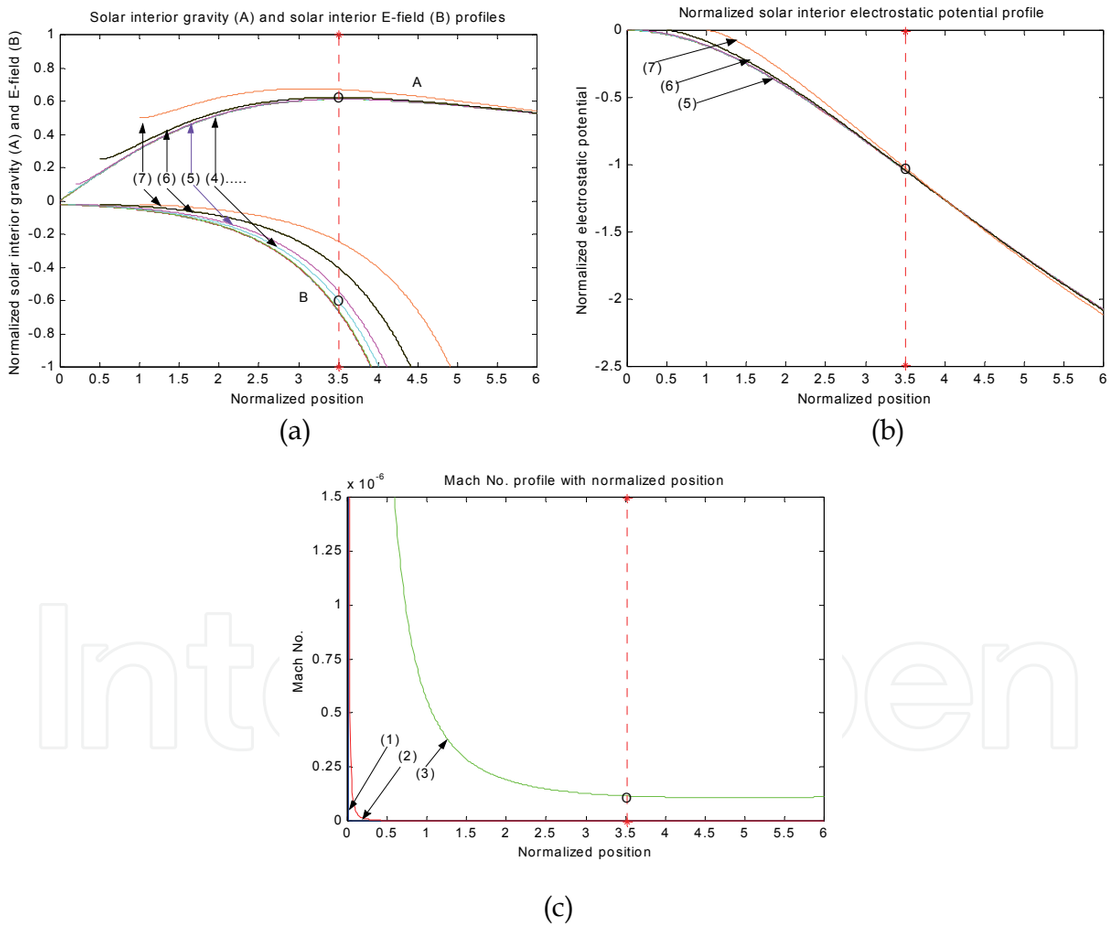

Fig. 9. Same as Fig. 8 but with the ion-to-electron temperature ratio $\varepsilon_T = 0.40$ and electrostatic potential $\theta_i = -0.001$ held fixed. The lines correspond to the cases with initial positions $\xi_i = 10^{-4}$ (graph 1), 10^{-3} (graph 2), 10^{-2} (graph 3), 10^{-1} (graph 4), 0.2 (graph 5), 0.5 (graph 6), and 1.0 (graph 7), respectively. The circled points indicate the most suitable choice of the solar surface values

This is to clarify that the GES-model is a quite simplified one in the sense that it does not include any role of magnetic forces, interplanetary medium or any other complications like rotations, viscosity, etc. It opens a new chapter for further study on the coupled system of the solar interior and exterior plasma flow dynamics.

According to GES-model, the normal acoustic modes of the global solar surface oscillations can be analyzed in terms of the local and global gravito-electrostatic plasma sheath oscillations governed by the basic principles of linear and nonlinear nonlocal theory of the Jeans collapse model [24-25] of charged dust clouds in plasma environment.

The magnified view of the Mach number variation in *transonic transition zone* of the SWP (Fig. 11c) indicates the existence of an extended region having almost uniform sonic flow speed. It can be deduced from Fig. 11c that the transonic point does not always coincide with the critical point. We define the critical point as a radial point (away from that defined solar surface) where the net force on the SWP ions, due to GES-induced *E*-field and external gravity due to total solar interior plasma mass, becomes almost zero.

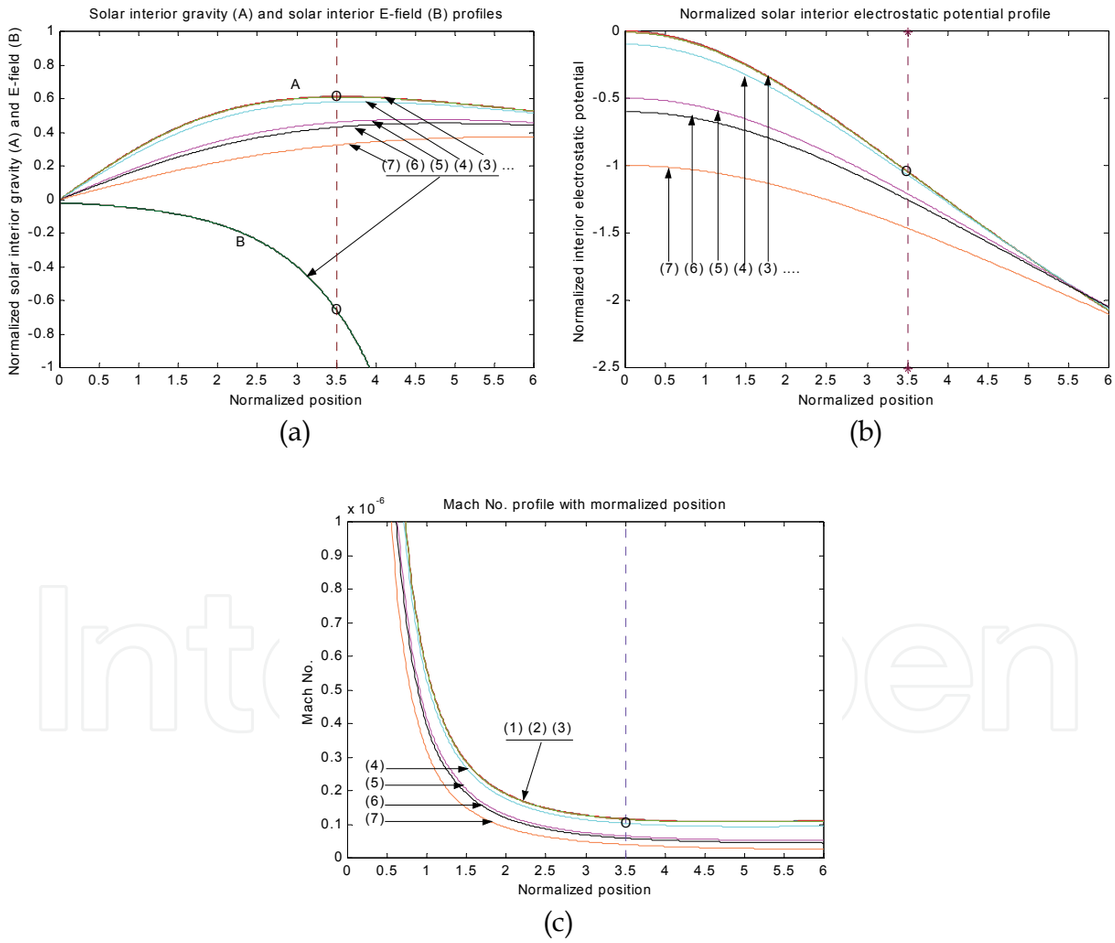

Fig. 10. Same as Fig. 8 but with the initial position $\xi_i = 0.01$ and ion-to-electron temperatue ratio $\varepsilon_T = 0.40$ held fixed. The lines correspond to the cases of $\theta_i = 0.0$ (graph 1), -0.001 (graph 2), -0.01 (graph 3), -0.1 (graph 4), -0.5 (graph 5), -0.6 (graph 6), and –1.0 (graph 7), respectively. The circled points indicate the most suitable choice of the solar surface values

Numerical solution in the GES-model reproduces the Parker model values of the SWP speed at 1 AU (Fig. 11a) for the numerically predetermined set of initial values of M_{SSB} ~10^{-7} and SWP ion-to-electron temperature ratio $\varepsilon_T = 0.0 - 0.1$. The estimated critical point for the transonic transition to occur $(r_c \sim 14 R_\Theta)$ differs from that $(r_c \sim 10 R_\Theta)$ in Parker's model. We find that the latter can be obtained with a choice of M_{SSB} ~10^{-6} (or larger than this by orders of magnitude) as an initial Mach value at the solar surface.

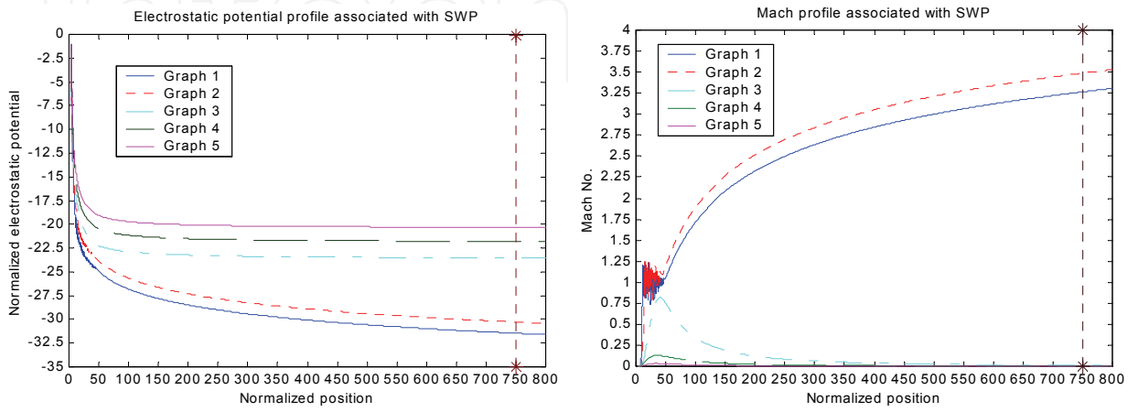

(a) (b)

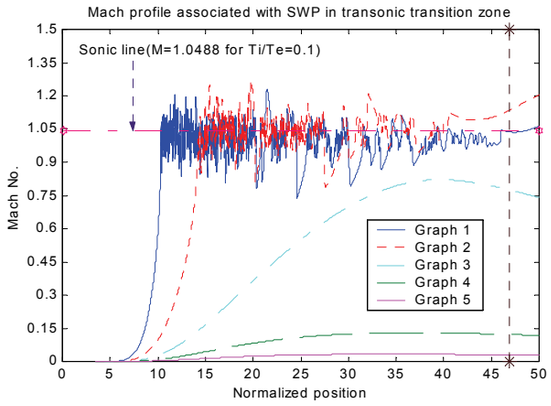

(c)

Fig. 11. Variation of normalized values of (a) speed M, (b) electrostatic potential θ, and (c) speed Min the transonic transition zone associated with SWP flow dynamics with respect to normalized position (ξ) from the solar surface boundary $(\xi_\Theta = 3.5)$ in magnified form. The predetermined solar surface boundary parameter values of $M_{SSB} \sim 10^{-7}$, $\theta_\Theta \sim -1.0$ and $a_0 = GM_\Theta / c_s^2 \lambda_J = 95$ are considered as the set of initial values. The lines correspond to the cases of ε_T = 0.0 (graph 1), 0.1 (graph 2), 0.2 (graph 3), 0.3 (graph 4), and 0.4 (graph 5), respectively. The critical distance lies at $\xi_c \cong 47.5$, which corresponds to a radial position of $r \sim 14 R_\Theta$ from the solar surface boundary

This is to clarify that the GES-model is a quite simplified one in the sense that it does not include any role of magnetic forces, interplanetary medium or any other complications like

rotations, viscosity, etc. It opens a new chapter for further study on the coupled system of the solar interior and exterior plasma flow dynamics.

According to GES-model, the normal acoustic modes of the global solar surface oscillations can be analyzed in terms of the local and global gravito-electrostatic plasma sheath oscillations governed by the basic principles of linear and nonlinear nonlocal theory of the Jeans collapse model [24-25] of charged dust clouds in plasma environment.

The magnified view of the Mach number variation in *transonic transition zone* of the SWP (Fig. 11c) indicates the existence of an extended region having almost uniform sonic flow speed. It can be deduced from Fig. 11c that the transonic point does not always coincide with the critical point. We define the critical point as a radial point (away from that defined solar surface) where the net force on the SWP ions, due to GES-induced *E*-field and external gravity due to the total SIP mass, becomes almost zero.

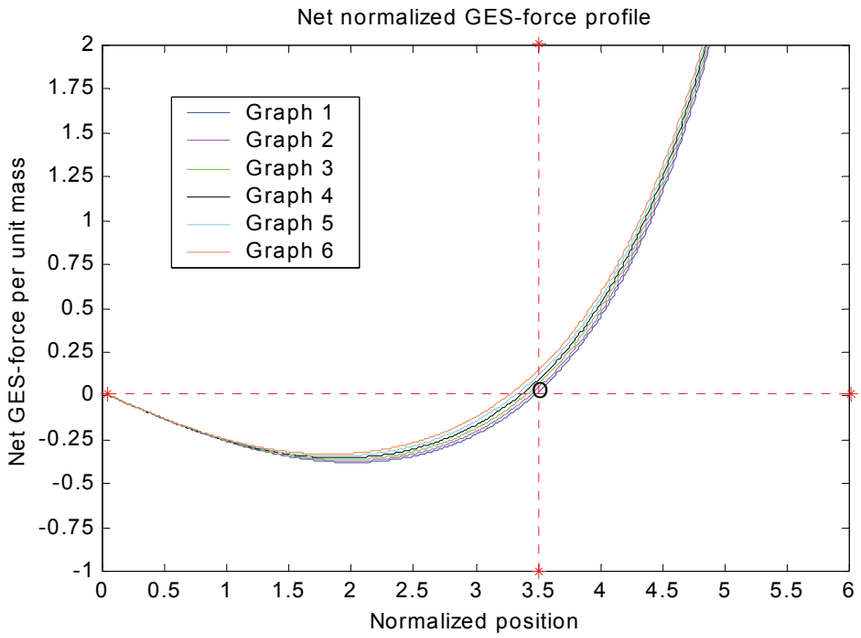

Fig. 12. Variation of net normalized GES force per unit mass associated with solar interior plasma flow dynamics with respect to normalized position (ξ) from the heliocentre $(\xi = 0)$. The initial position $\xi_i = 0.01$ and initial electrostatic potential $\theta_i = -0.001$ are held fixed. The lines correspond to the cases of ε_T = 0.5 (graph 1), 0.4 (graph 2), 0.3 (graph 3), 0.2 (graph 4), 0.1 (graph 5), and 0.0 (graph 6), respectively. The defined solar surface boundary is found to lie at a radial position $\xi_\Theta \sim 3.5$ for a more suitable choice of ε_T = 0.4-0.5 variations

Now, one can see that the sonic point for $\varepsilon_T = 0.0$ (graph 1 in Fig. 11c) falls around $\xi \cong 10$ whereas the transonic point for the same value of $\varepsilon_T = 0.0$ falls around the critical point $\xi_c \cong 47.5$. Similarly, one can see that the sonic point for $\varepsilon_T = 0.1$ (graph 2 in Fig. 11c) falls around $\xi \cong 15$ whereas the transonic point for the same value of $\varepsilon_T = 0.1$ falls around the non-critical point $\xi \cong 50$. From these numerical observations of the transonic transition region, one can clearly notice that an extended zone of about $40\lambda_J$ exists having almost a uniform sonic flow speed of the SWP between sonic and transonic points.

In this region, the inertia-induced acoustic excitation theory [5-12] may have potential applications provided it is improved with a proper inclusion of the solar gravity under nonlocal normal-mode analysis. Similar situations are likely to arise in laboratory plasmas of gravitationally sensitive multi-ion colloidal plasma systems [14-15, 24-25].
This is to point out that the intense acoustic fluctuations appearing in the Mach-profile (Fig. 11c) are merely the results of a numerical instability arising due to the mathematically indeterminate situations localized mainly near the sonic speed. These fluctuations, however, are found to disappear beyond the critical distance. Physically, however, the physical appearance of such indeterminate structures in the graphical plots is because of some chaotic interference and intermittency of acoustic background fluctuations in the emitted SWP. It may produce some dissipative effects in course of the electrodynamical process of the electrodynamical interaction of the SWP particles with background particles of ambient stellar atmosphere.

5.6 Comparison with exospheric model

Exospheric model [38-39] is a simple kinetic model for the solar coronal plasma expansion. This model assumes that beyond a given altitude termed as the '*exobase*' from the SSB, binary collisions between the SWP-particles are negligible. The coronal plasma expansion is believed to occur due to thermal evaporation of the hot protons that have velocity exceeding the escape velocity so as to cross over the barrier of the external solar gravitational field. The generalized model [19-23] considers the non-Maxwellian velocity distribution function for the coronal plasma electrons.
Of course, this model has succeeded to explain the observation of the high speed SWP. This model indeed explains the high speed SWP without requiring any additional source to heat the coronal plasma electrons. In this model, the exobase is defined by the condition that the density scale length equals the mean free path of the SWP particles. Due to the complexities of coronal based physics and multiplicities of plasma species different exobases are likely to coexist. Moreover, the appropriate electrostatic potential is determined by applying the approximations of both local quasi-neutrality and zero current. Of course, this model has succeeded in explaining the observation of the high-speed SWP. But according to our model calculations, the zero-current approximation of the exospheric model seems to be valid only on large scales but not near and above the SSB.
By our GES-model analyses, a finite electron-dominated [10-11] current with a positive finite divergence exists on the solar interior scale for $d\theta/d\xi < 0$. Immediately after the SSB, i.e., on the unbounded scale of the SWP, a divergence-free current exists. This seems to exhibit a discontinuous behavior. How to resolve this? In reality electron temperature has variable profiles on both the bounded and unbounded scales. Probably a self-consistent profile of two distinct electron temperatures on two regions of bounded and unbounded scales separately may resolve the interfacial transition problem of the proposed two-scale theory of the GES-associated solar plasma current system.
According to our GES theory and model calculations, the zero-electric current approximation of exospheric model calculations [38-39] requires further review. The appropriate electrostatic potential estimate from numerical analysis emphasizes that the zero electric current approximation is an outcome of the GES model on the large scale of the SWP. Now the question may naturally arise, "What happens to the SWP current after the transonic transition?" It seems that the electron-dominated electric current dissipates mainly through a channel of inertial resistance of the plasma ions due to solar gravity as a barrier.

The other dissipation channels of the electric current may be through the SWP heating generation of fluctuations in thermal noise level, etc. The uniform flow region of the SWP is, in addition, found to have a large number of conservation rules [11] under the lowest order inertial correction of the thermal electrons in the solar plasma system approximately from applied mathematical point of view. The details of the associated physical mechanism and fluctuations will be communicated to somewhere else.

5.7 Comments

Before we conclude with any physical comment, we must admit that the neglect of collisional dissipation and deviation from a Maxwellian velocity distribution of the plasma particles is not quite realistic. But our GES model under these simple approximations may provide quite interesting results. For example, it provides deep physical insight into the interconnection between the Sun and the SWP. The violation of the zero-current approximation is indeed noted in the neighborhood of the SSB and above. Of course, the zero current approximation seems to be satisfied beyond the transonic region. This conclusion is based on the well-known condition of the floating surface boundary in basic plasma sheath physics.

An estimated value $\lambda_{De}/\lambda_J \sim 10^{-20}$ of the ratio of the solar plasma Debye length and the Jeans length of the total solar mass justifies the quasi-neutral behavior of the solar plasma on both the bounded and unbounded scales.

Applying the spherical capacitor charging model, the coulomb charge on the SWP at a distance of ~ 1 AU comes out to be . For rotation frequency of the solar plasma system corresponding to the mean angular frequency about the centre of the system (Gunn 1931), the mean value of the strength of the solar magnetic field associated with the SWP in our model analysis is estimated as $\langle |B_{SWP}| \rangle = 4\pi^2 Q_{SWP} f_{SWP} \sim 3.01 \times 10^{11} T$. This is obviously considerably higher for producing any significant effects on the dynamics of the SWP particles. Thus the effects of the magnetic field are not ignorable for the SWP particles due to the significantly strong Lorentz force, which is now estimated to be $F_L = e(v_0 \times B_{SWP}) \approx 1.64 \times 10^{-2} N$ corresponding to a supersonic flow speed $v_0 \sim 340.00\, km\, s^{-1}$. Thus the Lorentz force may have some remarkable effect on the SWP particles and hence, may not justifiably neglected for the unbounded scale description. It justifies the convective and circulation dynamics to be considered in that context. Therefore our unmagnetized plasma approximation may not prove well justified in our GES model configuration for the SWP flow dynamics description. Although collision processes are dominant in the realistic solar interior [2, 39-44], collisionless models [2, 39] are also equally useful for the solar plasma description. Thus our collisionless model approximation for mathematical simplicity may be justified here. In our GES model, the calculated values of the mean free paths for the solar plasma electrons, $\lambda_e \sim 1.50 \times 10^{198} m$ and for ions, $\lambda_i \sim 3.05 \times 10^{132} m$ justify the collisionless model approximation. This approximation holds good justifiably under the fulfillment of the validity condition $\lambda_e, \lambda_i >> \lambda_J$.

One can note that the SIP electron temperature, specified by T_{e1}, differs from (exceeds) the SWP electron temperature specified T_{e2} by one order of magnitude. This is discussed already discussed above. It simply means the SWP has been relatively cooled. It is quite natural for expanding plasma gas to be cool. This is to further comment that these two different electron temperatures are considered constant over their respective scales.

Actually, a discontinuity exists at the interface of the bounded and unbounded scales. This is an open problem to resolve.

Let us clarify once again that equalizing the maximum value of the numerically determined solar self-gravity with the standard value specifies the SIP electron temperature. Similarly, the appropriate choice of the defined constant a_0 specifies the SWP electron temperature, which ensures that a transonic solution of the SWP dynamics exists. Now, with this simplified treatment our theoretical model calculations yield the following conclusions.

1. Contrary to the general belief that the SWP emerges from the SSB, our theory provokes us to argue that the genesis of the subsonic origin of the SWP at the SSB in fact lies in the SIP dynamics. It is governed by the basic principles of the GES formation near the SSB and beyond. The surface boundary is located at a radial distance defined by $\xi \sim 3.5$ (Figs. 8–10) from the heliocentric origin. This specific location in the plots (Figs. 8a, 9a, and 10a) is marked by a vertical line with small circles.
2. Thereafter, the outward moving SIP forms the SWP with a highly subsonic speed at the SSB. Initially the outward acceleration of the SWP is quite rapid allowing a *transonic transition* solution to exist for a specific choice of $\varepsilon_T = 0.0 - 0.1$ (Fig. 11a). This occurs as a consequence of the predominantly self-consistent electric field associated with the SWP (Fig. 11b). It produces a *transonic transition region* of sufficient length scale with the critical point lying at about $14R_\Theta$ (Fig. 11c) from the SSB.
3. It is noted that initially the gravitational potential barrier decelerates the SIP dynamics rapidly. As soon as the *E*-field of the SIP origin gathers sufficient strength, an outward flow occurs with a reduced minimum speed of $M_{SSB} \sim 10^{-7}$ (Figs. 8c, 9c, 10c) at the SSB defined by the quasi-hydrostatic equilibrium condition at a point of the maximum solar gravity, as clearly depicted in Fig. 12. This figure clearly shows the strong solar self-gravity up to the solar boundary and relatively weaker strength of the solar external gravity beyond the boundary.
4. According to our model calculations, the SSB behaves as a negatively biased grid with a bias potential of about 1 kV. The surface draws a finite current dominated by the thermal electrons and flows towards the surface. As a result, the solar surface oscillations may naturally be attributed to the resulting consequences of the GES oscillations. Under the neutral ideal gas approximation of the SIP, this property cannot be deduced.
5. We therefore conclude that our GES-based model may be useful to study the properties of the SSB and the properties of the slow speed SWP. Of course, the properties of the high speed SWP description under our model will require a kinetic treatment as already reported by previous workers in the case of the exospheric model.

A few more reminders are in order:

1. The exact location of the SSB and that of 1 AU distance as specified in Figs. 8-12 on the normalized scale are estimated for the normalization factor, which is, decided by the SIP parameters.
2. In the absence of magnetic field in our model approach, the Lorenz force term is absent, but it will be needed for further improvements under the fluid and/or kinetic regime to see the realistic dynamics of the solar plasma system. However, the estimated mean

value of the solar magnetic field $\langle |B_{SIP}| \rangle \sim 7.53 \times 10^{-11} T$ in the SIP justifies and supports our unmagnetized plasma approximation in the present context.

3. The GES-model is a useful theoretical construct with which to study SWP dynamics in terms of solar interior dynamical behavior (generator of the SWP) through active dynamical coupling processes of solar exterior regions in the light of localized electric space charge effects.

Finally, it is important to comment that the further improvements and modifications to the model will be needed to make it more realistic for actual SWP conditions. These form the basic problems of future research on the GES model. The genesis of the SWP is now found to be associated with the coupling of the SIP potential and self-gravitational potential of the SIP mass. We finally argue that the lines of communications should be kept open between theorists and observers and solar and stellar physicists, and more importantly also between the solar and plasma physics communities, in order to further the study of stellar wind plasmas. Ours is a first step, albeit very simplified and external-field free and ideal, in this particular direction. We have tried to provide an integrated theoretical outlook on the SIP dynamics on the bounded scale, and SWP on the unbounded scale. This model could further be useful to study the properties of the helio-seismic dynamics of the Sun and other stars [36-37] too.

5.8 Overall summary

The presented chapter reviews the latest findings of normal acoustic mode analyses through different types of transonic plasma equilibrium models [5-12] under the lowest order inertial correction of plasma thermal species. Different types of acoustic resonances are observed in transonic plasma equilibria depending on different plasma inertial ions. The linear analyses show the graphical nature of the associated resonance poles. This implies that transonic plasma is an unstable zone, which is rich in wide range spectra of acoustic wave fluctuations. The acoustic wave kinetics in the nonlinear normal mode analyses in different types of plasmas [8-9, 12, 26] is describable by a linear source driven KdV (*d*-KdV) equation. After integration, it shows two distinct classes of soluations, i. e., solitons and oscillatory shocks. The fundamental condition to observe inertia-induced (ion) acoustic wave resonant excitation is that the ion flow speed must be uniform. Accordingly, the same applies to the solar wind dynamics [10-11, 35-41] in self-gravitating plasma systems as well. A large number of conservation laws of applied mathematical significance associated with the *d*-KdV flow dynamics are also pointed out [9] in transonic plasma domain in different situations including solar plasma. Of course, convective and circulation dynamics which are the primary sources of magnetic field [41], are neglected throughout for simplicity. Similar observations of acoustic kinetics of the formation of soliton-type structures are also found in self-gravitating dust molecular clouds in presence of partially ionized dust grains through the active mechanism of gravito-acoustic coupling processes [27]. Some future scopes including realistic sources of acoustic perturbation of the presented analyses are also pointed out in brief.

Very similar to Geoseismology dealing with the Earth's interior through the various seismic (acoustic) waves produced during the earthquakes, Helioseismology is the study of the various linear and nonlinear surface waves and oscillations of solar origin (like *p-mode*, and *f-mode*) to measure the internal structure and dynamics of the Sun [36-44]. The acoustic dynamics in the Sun (or Star) is understandable by considering it to have a resonant cavity like an organ pipe in which acoustic waves are trapped (by reflections or refractions) [41].

One of the earliest studies of solar oscillations and fluctuations established that the power spectrum of the Sun's full disk contained a multitude of Doppler shift peaks between 2.5 mHz - 4.5 mHz [36-37 and references therein]. The Global Oscillation Network Group (GONG), Stellar Observations Network Group (SONG), Helio- and Asteroseismology (HELAS) Network, and Birmingham Solar Oscillations Network (BiSON) are examples of recent studies being undertaken to measure these surface oscillations through space and ground based remote-sensing observations [36-37, 44]. Michelson Doppler Imager (MDI) onboard Solar and Heliospheric Observatory (SOHO) and recently, Helioseismic Magnetic Imager (HMI) onboard Solar Dynamics Observatory (SDO) also measure these oscillations from space [36-37, 41, 44]. Significant power has been observed at frequencies ranging from 1.4 mHz to 5.6 mHz, corresponding to periods of 3 to 12 minutes. They are called '*5 minute oscillations*' due to their dominant mean period [44]. Besides, the behavior of the solar intermediate-degree modes (during extended minimum) is also investigated to explore the time-varying solar interior dynamics with the help of contemporaneous helioseismic GONG and MDI data [44]. The basic physics behind these helioseismic and helioacoustic observations (*in situ*) reported in the literature, however, needs to be more clearly understood in a broader horizon. Moreover, there are many more experimental observations [3, 35-44] on seismic activities that will require self-gravitating plasma wave theory for further development of our stability analyses and seismic diagnostics. In conclusion, we strongly believe that the presented mathematical strategies and techniques of linear and nonlinear acoustic mode analyses amidst more realistic plasma-boundary interaction processes may have some potential applications in such future helio- and astero-seismic directions.

6. Acknowledgements

I am thankful to Ms. Sandra Bakic, Publishing Process Manager, InTech - Open Access Publisher, for the invitation, chapter proposal and continuous cooperation. I am also thankful to each and everybody of the InTech family whoever involved for extending cooperation. Lastly, I gratefully recognize the Intech Editorial Board for giving me this rare opportunity to publish this chapter in the book "Acoustic Wave/Book 2" without any article processing charge.

7. References

[1] B. W. Tillery, *Physical Sciences* (8th Edition, McGraw-Hill 2009), Ch. 5, pp. 115-134.
[2] F. F. Chen, *Introduction to Plasma Physics and Controlled Fusion* (Plenum Press, New York and London, 1988), Ch.1, pp. 1-17.
[3] S. R. Cranmer, *Space. Sci. Rev.* 101, 229 (2002).
[4] M. Lakshamanan and S. Rajasekhar, *Nonlinear Dynamics: Integrability, Chaos, and Patterns* (Springer-Verlag Heidelberg 2003), Ch. 11-14, pp. 341-454.
[5] C. B. Dwivedi and R. Prakash, *J. Appl. Phys.* 90, 3200 (2001).
[6] P. K. Karmakar, U. Deka and C. B. Dwivedi, *Phys. Plasmas* 12, 032105 (2005).
[7] P. K. Karmakar, U. Deka and C. B. Dwivedi, *Phys. Plasmas* 13, 104702 (1) (2006).
[8] P. K. Karmakar and C.B. Dwivedi, *J. Math. Phys.* 47, 032901(1) (2006).
[9] P. K. Karmakar, *J. Phys.: Conf. Ser.* 208, 012059(1) (2010).
[10] C. B. Dwivedi, P.K. Karmakar and S.C. Tripathy, *Astrophys. J.* 663 (2), 1340 (2007).
[11] P. K. Karmakar, *J. Phys.: Conf. Ser.* 208, 012072(1) (2010).

[12] U. Deka, A. Sarma, R. Prakash, P. K. Karmakar and C. B. Dwivedi, *Phys. Scr*. 69, 303 (2004).
[13] P. Mora, *Phys. Rev. Lett*., 90, 185002-1 (2003).
[14] C. B. Dwivedi, *Pramana-J. Phys*. 55, 843 (2000).
[15] C. B. Dwivedi, *Phys. Plasmas* 6, 31 (1999).
[16] M. S. Sodha and S. Guha, *Advances in Plasma Physics*, edited by A. Simon and W. B. Thompson (Wiley, New York, 1971) vol. 4.
[17] C. K. Goertz, *Rev. Geophys*. 27, 271 (1989).
[18] F. Verheest, *Space Sci. Rev*. 77, 267 (1996).
[19] H. Thomas, G. E. Morfill, V. Demmel, J. Goerce, B. Feuerbacher and D. Mohlmann, *Phys. Rev. Lett*. 73, 652 (1994).
[20] G. S. Selwyn, J. E. Heidenreich and K. L. Haller, *Appl. Phys. Lett*. 57, 1876 (1990).
[21] L. Boufendi, A. Bouchoule, P. K. Porteous, J. Ph. Blondeau, A. Plain and C. Laure, *J. Appl. Phys*. 73, 2160 (1993).
[22] A. Gondhalekar, P. C. Stangeby and J. D. Elder, *Nucl. Fusion* 34, 247 (1994).
[23] B. N. Kolbasov, A. B. Kukushkin, V. A. Rantsev Kartinov, and P. V. Romanov, *Phys. Lett. A* 269, 363 (2000).
[24] N. N. Rao, P. K. Shukla and M. Y. Yu, *Planet. Space Sci.* 38, 345 (1990).
[25] P. K. Shukla, *Waves in dusty, solar wind and space plasmas,* (AIP Conference proceedings, Leuven, Belgium) 537, 3 (2000).
[26] P. K. Karmakar, *Pramana- J. Phys.* 68, 631 (2007).
[27] P. K. Karmakar, *Pramana- J. Phys.* 76 (6), 945 (2011).
[28] J. P. Goedbloed, R. Keppens and S. Poedts, S*pace Sci. Rev.* 107, 63 (2003).
[29] S. P. Kuo and D. Bivolaru, *Phys. Plasmas* 8 (7), 3258 (2001).
[30] K. Itoh, K. Hallatschek and S-I Itoh, *Plasma Phys. Control. Fusion* 47, 451 (2005).
[31] I. Ballai, *PADEU* 15, 73 (2005).
[32] I. Ballai, E. Forgacs and A. Marcu, *Astron. Nachr*. 328 (8), 734 (2007).
[33] P. K. Shukla and A. A. Mamun, *New J. Phys.* 5, 17.1 (2003).
[34] M. Khan, S. Ghosh, S. Sarkar and M. R. Gupta, *Phys. Scr.* T116, 53 (2005).
[35] M. S. Ruderman, *Phi. Trans. R. Soc. A*, 364, 485 (2006).
[36] W. J. Chaplin, *Astron. Nachr*. 331 (9), 1090 (2010).
[37] J. C. Dalsgaard, *Astron. Nachr*. 331 (9), 866 (2010).
[38] J. Lemaire and V. Pierrard, *Astrophys. Space Sci.* 277, 169 (2001).
[39] E. Marsch, *Liv. Rev. Solar Phys.* 3, 1 (2006) (http: //livingreviews.org/lrsp-2006-1).
[40] U. Narain and P. Ulmschneider, *Space Sci. Rev.* 75, 453 (1996).
[41] A. Nordlund, R. F. Stein and M. Asplund, *Living Rev. Solar Phys.* 6, 2 (2009) (http: //livingreviews.org/lrsp-2009-2).
[42] R. Gunn, *Phys. Rev*. 37, 983 (1931).
[43] V. M. Nakariakov and E. Verwichte, *Living Rev. Solar Phys.* 2, 3 (2005) (http: //livingreviews.org/lrsp-2005-3).
[44] S. C. Tripathy, F. Hill, K. Jain and J. W. Leibacher, *Astrophys. J.* 711, L84 (2010).

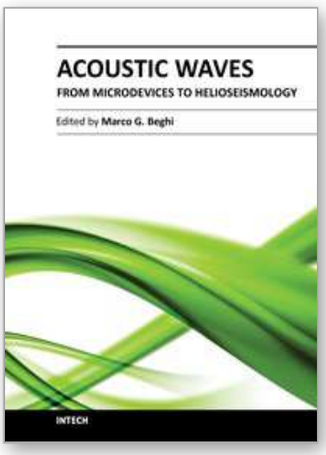

Acoustic Waves - From Microdevices to Helioseismology

Edited by Prof. Marco G. Beghi

ISBN 978-953-307-572-3
Hard cover, 652 pages
Publisher InTech
Published online 14, November, 2011
Published in print edition November, 2011

The concept of acoustic wave is a pervasive one, which emerges in any type of medium, from solids to plasmas, at length and time scales ranging from sub-micrometric layers in microdevices to seismic waves in the Sun's interior. This book presents several aspects of the active research ongoing in this field. Theoretical efforts are leading to a deeper understanding of phenomena, also in complicated environments like the solar surface boundary. Acoustic waves are a flexible probe to investigate the properties of very different systems, from thin inorganic layers to ripening cheese to biological systems. Acoustic waves are also a tool to manipulate matter, from the delicate evaporation of biomolecules to be analysed, to the phase transitions induced by intense shock waves. And a whole class of widespread microdevices, including filters and sensors, is based on the behaviour of acoustic waves propagating in thin layers. The search for better performances is driving to new materials for these devices, and to more refined tools for their analysis.

How to reference

In order to correctly reference this scholarly work, feel free to copy and paste the following:

P. K. Karmakar (2011). Acoustic Wave, Acoustic Waves - From Microdevices to Helioseismology, Prof. Marco G. Beghi (Ed.), ISBN: 978-953-307-572-3, InTech, Available from: http://www.intechopen.com/books/acoustic-waves-from-microdevices-to-helioseismology/acoustic-wave

INTECH
open science | open minds

InTech Europe
University Campus STeP Ri
Slavka Krautzeka 83/A
51000 Rijeka, Croatia
Phone: +385 (51) 770 447
Fax: +385 (51) 686 166
www.intechopen.com

InTech China
Unit 405, Office Block, Hotel Equatorial Shanghai
No.65, Yan An Road (West), Shanghai, 200040, China
中国上海市延安西路65号上海国际贵都大饭店办公楼405单元
Phone: +86-21-62489820
Fax: +86-21-62489821

IntechOpen